The FEBS Journal

FEBS PRESS science publishing by scientists

Serine metabolism during differentiation of human iPSC-derived astrocytes

Farida Tripodi[1], Zoraide Motta[2], Giulia Murtas[2], Valentina Rabattoni[2], Simona Nonnis[3], Francesca Grassi Scalvini[3], Anna Maria Rinaldi[4], Roberto Rizzi[5,6], Claudia Bearzi[5,7], Beatrice Badone[1,*], Silvia Sacchi[2], Gabriella Tedeschi[3,8], Elisa Maffioli[3], Paola Coccetti[1] and Loredano Pollegioni[2]

1 Department of Biotechnology and Biosciences, University of Milano-Bicocca, Italy
2 Department of Biotechnology and Life Sciences, University of Insubria, Varese, Italy
3 DIVAS, Department of Veterinary Medicine and Animal Science, University of Milano, Italy
4 Department of System Medicine, University of Rome "Tor Vergata", Italy
5 Fondazione Istituto Nazionale di Genetica Molecolare, Milan, Italy
6 Department of Medical-Surgical Science and Biotechnologies, University of Rome La Sapienza, Italy
7 Institute for Biomedical Technologies, National Research Council of Italy (ITB-CNR), Milan, Italy
8 CIMAINA, University of Milano, Italy

Keywords
amino acid metabolism; D-serine; metabolomics; neurotransmission; proteomics

Correspondence
E. Maffioli, DIVAS, Department of Veterinary Medicine and Animal Science, University of Milano, Milan 20121, Italy
Tel: +390250334544
E-mail: elisa.maffioli@unimi.it
P. Coccetti, Department of Biotechnology and Biosciences, University of Milano-Bicocca, Milan 20126, Italy
Tel: +390264483521
E-mail: paola.coccetti@unimib.it
and
L. Pollegioni, Department of Biotechnology and Life Sciences, University of Insubria, Varese 21100, Italy
Tel: +390332421506
E-mail: loredano.pollegioni@uninsubria.it

Present address
*Sophion Bioscience A/S, Baltorpvej 154, 2750, Ballerup, Denmark

Astrocytes are essential players in development and functions, being particularly relevant as regulators of brain energy metabolism, ionic homeostasis and synaptic transmission. They are also the major source of L-serine in the brain, which is synthesized from the glycolytic intermediate 3-phosphoglycerate through the phosphorylated pathway. L-Serine is the precursor of the two main co-agonists of the *N*-methyl-D-aspartate receptor, glycine and D-serine. Strikingly, dysfunctions in both L- and D-serine metabolism are associated with neurological and psychiatric disorders. Here, we exploited a differentiation protocol, based on the generation of human mature astrocytes from neural stem cells, and investigated the modification of the proteomic and metabolomic profile during the differentiation process. We show that differentiated astrocytes are more similar to mature rather than to reactive ones, and that axogenesis and pyrimidine metabolism increase up to 30 days along with the folate cycle and sphingolipid metabolism. Consistent with the proliferation and cellular maturation processes that are taking place, also the intracellular levels of L-serine, glycine, threonine, L- and D-aspartate (which level is unexpectedly higher than that of D-serine) show the same biosynthetic time course. A significant utilization of L-serine from the medium is apparent while glycine is first consumed and then released with a peak at 30 days, parallel to its intracellular level. These results underline how metabolism changes during astrocyte differentiation, highlight that D-serine synthesis is restricted in differentiated astrocytes and provide a valuable model for developing potential novel therapeutic approaches to address brain diseases, especially the ones related to serine metabolism alterations.

Abbreviations
CNS, central nervous system; DAAO, D-amino acid oxidase; DE, differentially expressed; ECAR, extracellular acidification rate; ECM, extracellular cell matrix; EE, exclusively expressed; GC, gas chromatography; hiPSC, human induced pluripotent stem cells; HPLC, high-performance liquid chromatography; HRP, horseradish peroxidase; LC, liquid chromatography; LFQ, label-free quantification; MS, mass spectrometry; NMDA, *N*-methyl-D-aspartate; NSCs, neural stem cells; OCR, oxygen consumption rate; PHGDH, phosphoglycerate dehydrogenase; PLS-DA, partial least-squares discriminant analysis; PP, phosphorylated pathway; PPP, pentose phosphate pathway; PSAT1, phosphoserine aminotransferase 1; PSP, phosphoserine phosphatase; SR, serine racemase; TCA cycle, tricarboxylic acid cycle.

Farida Tripodi and Zoraide Motta contributed equally to this article

(Received 14 November 2022, revised 5 April 2023, accepted 10 May 2023)

doi:10.1111/febs.16816

Introduction

Astrocytes are the most abundant cell types in the central nervous system (CNS) [1] with extraordinary morphological and functional heterogeneity [2]. Neural stem cells (NSCs) in the neuroepithelium of the developing CNS and in discrete areas of adult brains (neurogenic niches) continue to differentiate into committed neuronal subtypes, such as neurons, astrocytes and oligodendrocytes [3]. Besides providing structural support, they are crucially engaged in neuronal pathfinding, as well as in the control of trafficking across the blood–brain barrier [4].

Astrocytes also play a key role in numerous functions including glutamate, ion and water homeostasis, defence against oxidative stress, energy storage and supply, mitochondria biogenesis and tissue healing. They secrete a large number of molecules thus being considered the major secretory cells in the CNS. Indeed, they release neurotransmitters, modulators, peptides, hormones, trophic growth factors and metabolites. Secreted molecules dynamically participate in synapse formation, function, elimination, plasticity, differentiation, neuronal growth, survival, as well as in the regulation of blood flow in the brain [5–8]. Astrocytes are also main regulators of brain metabolism. Their anatomical position between blood vessels and neurons makes them a crossing point for efficient glucose uptake from the blood. Astrocytic glucose-6-phosphate can be processed into three metabolic pathways: aerobic glycolysis, pentose phosphate pathway (PPP) and storage as glycogen. One major function of aerobic glycolysis is to maintain high levels of glycolytic intermediates to support anabolic reactions in cells [9].

On this side, the nonessential amino acid L-serine is produced through the re-routing of the glycolytic intermediate 3-phosphoglycerate into the phosphorylated pathway (PP). The PP is a short metabolic sequence consisting of three consecutive and ordered enzymatic reactions catalysed by the following enzymes: phosphoglycerate dehydrogenase (PHGDH), mainly expressed in astrocytes [10], phosphoserine aminotransferase 1 (PSAT1) and phosphoserine phosphatase (PSP) [11]. L-Serine, primarily found in astrocytes, is a major carbon source in the one-carbon metabolic pathway; it is also required for the biosynthesis of proteins, phosphoglycerides, glycerides, nucleotides, sphingolipids, phosphatidylserine and methylenetetrahydrofolate [11]. Notably, L-serine is the precursor of the two main co-agonists of *N*-methyl-D-aspartate (NMDA) receptors: glycine and D-serine (D-Ser). The latter is synthesized from L-serine by the enzyme serine racemase (SR), upon the shuttling of the precursor in neurons, where SR is mainly expressed [12]. Dysfunctions in D-Ser metabolism and the consequent alteration in its brain level have been associated with neurological diseases and psychiatric disorders. Of note, mutations in genes coding for enzymes of the PP pathway are associated with several neurological disorders [11], indicating the relevance of serine synthesis for brain functionality.

Furthermore, PHGDH is essential for nucleotide metabolism and associated events, like proliferation and cellular energy source, as elegantly demonstrated both *in vitro* in HTC16 cells [13] and *in vivo* in PHGDH knockout mice. The latter manifests a severe impairment of neurogenesis associated with a significant dysregulation of genes involved in the cell-cycle progression [14]. Thus, altered expression levels of the PP enzymes, and in particular of PHGDH, are expected to contribute not only to a reduced proliferation [13] but also to distorted glial-neuron communication and eventually to NMDA receptor function impairment, as well as to impairment of multi-faced functions linked to one-carbon metabolic pathway. This latter comprises three vital biochemical cycles: the folate cycle (glycine and serine power mitochondrial enzymes via purine production), the methionine cycle (*S*-adenosylmethionine is the major methyl donor regulating methylation status of nucleic acids and histone proteins, among others) [15] and the trans-sulfuration pathway (essential for the synthesis of glutathione and crucial for deactivating radicals and reactive oxygen species molecules) [16]. The expression levels of the PP

enzymes have been recently investigated to shed light on brain metabolism during healthy ageing vs Alzheimer's disease onset [17,18].

Since astrocytes play such an important role in brain homeostasis and functioning, their impairment is implicated in the pathogenesis of several neurological diseases [19]. In response to pathological insults, they undergo molecular, morphological and functional changes [20], and during these processes, they can play either neuroprotective or neurotoxic roles. For these reasons, modelling astrocytes and their interactions with neurons is considered of paramount importance from both fundamental and translational perspectives. Although most studies on astrocytes have been performed using mouse models, important differences between human and mouse astrocytes have been reported [21]. Therefore, the generation of astrocytes from NSCs has attracted much attention recently. Although NSCs and astrocytes share common phenotypic and functional characteristics [22,23], their transcriptomic and proteomic profiles show several differences. Fluxomic studies also indicate the downregulation of central carbon metabolism in murine NSC-derived astrocytes [24]; transcriptional and functional differences between human and murine astrocytes have been reported [25].

In this regard, we exploited the potential of human fibroblasts reprogrammed to induced pluripotent stem cells (hiPSC) and further differentiated in NSC and then into astrocytes, with the ambitious goal to provide an insight into the cellular processes timely involved in the differentiation programme. The molecular understanding of astrocyte differentiation from NSCs is an important aspect to consider for modulating astrocyte physiology in human pathologies and for developing potential therapeutic strategies. Thus, to get a complete picture of the changes that occur during astrocytes differentiation, we resorted to an integrated multi-omic approach to evaluate how the proteomic and metabolic profile progress at different times of differentiation of NSC-derived human astrocytes, with a particular focus on the PP pathway.

Results

Generation and functional characterization of hiPSC-derived astrocytes

We generated a human induced pluripotent stem cell line from human fibroblast [BJ (ATCC CRL-2522)] utilizing SENDAI virus carrying the embryonic genes for OCT4 (octamer-binding transcription factor 4), SOX2 (SRY-Box transcription factor 2), KLF4 (Kruppel like factor 4) and cMYC (MYC proto-oncogene). Stem cells pluripotency was verified using sets of established markers and different techniques: (a) OCT4 and SSEA4 (stage-specific embryonic antigen-4) by immunofluorescence analysis; (b) OCT4, SOX2 and NANOG (Nanog homeobox) genes by quantitative real-time PCR (qRT-PCR) (Fig. 1A,B).

The hiPSC cell line was differentiated using the Neural Induction Medium and expanded. The resulting NSC colonies expressed typical markers, including nestin, SOX2 and PAX6 as assessed by immunofluorescence staining (Fig. 1C) and nestin, PAX6 and SOX1, as evaluated by qRT-PCR (Fig. 1D). A monolayer protocol was then used to differentiate NSCs into astrocytes combining low initial seeding density and reduced serum exposure (1%). We first tracked astrocytes at different times of differentiation (Days 2, 15, 30, 40 and 56) by western blot analysis for two classical astrocytes markers, GFAP (glial fibrillary acidic protein) and EAAT1 (excitatory amino acid transporter 1) [19], as well as for SOX2, as a marker of NSC. In line with previously reported studies [26,27] EAAT1 and GFAP protein levels increased gradually, with the highest level detected between 30 and 56 days, while SOX2 was progressively downregulated over time (Fig. 1E). Cell growth was fast at the beginning of the differentiation process but slowed down after 20 days and finally stopped after 30 days, which corresponds to the reported stage of mature astrocytes by this protocol (Fig. 1F). Coherently, quantification analyses performed at 30 days showed that almost all cells were $S100\beta^+$ (S100 calcium-binding protein B) and $EAAT1^+$, and that the proportion of $GFAP^+$ cells increased from 43% to 75% from Days 30 to 56 (Fig. 1G–I). The neuronal marker β3 tubulin was undetectable at Day 30, indicating that there was no contamination of neurons (Fig. 1H).

To further investigate whether additional astrocyte-enriched proteins [19] were expressed in a time-dependent manner, the proteome of hiPSC-derived astrocytes at the different differentiation time points was characterized by a quantitative shotgun label-free proteomic approach (as depicted in Fig. 2A) to identify and quantify expressed proteins (Fig. 2B,C; Table S1A–F). Furthermore, to verify that the prolonged *in vitro* differentiation protocol did not induce an activated phenotype, potential markers of reactive astrocytes [20,28,29] were also evaluated (Table S2). Many of them were identified at all differentiation time points and the differences in their expression level were not statistically significant with the only exception of CD44, as well as GFAP, vimentin (VIM) and tenascin (TNC), widely used as markers of reactive astrocytes [29], which strongly increased at Day 56 compared with Day 30

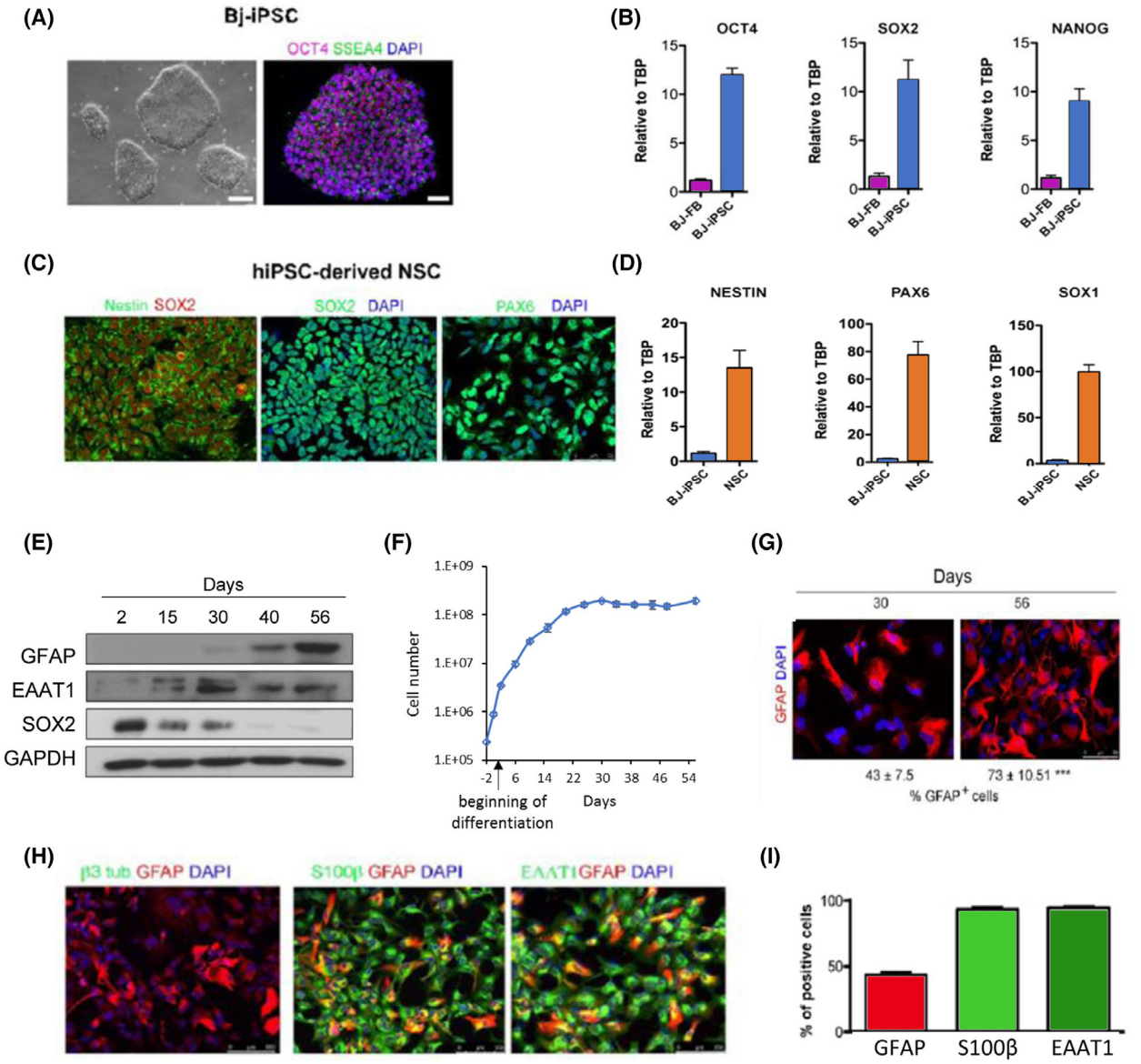

Fig. 1. Characterization of human fibroblast-derived hiPSCs (Bj-iPSC), Bj-iPSC-derived-NSCs (NSCs) and hiPSC-derived astrocytes. (A) Morphology of Bj-iPSC cultured in feeder-free conditions (left panel). Scale bar: 100 μm. Immunofluorescence labelling for the expression of the pluripotency markers in Bj-iPSC (SSEA4 and OCT4); nuclei were stained with DAPI (blue, right panel). Scale bar: 50 μm. (B) Gene expression analysis by qPCR in BJ-FB and BJ-IPSC of OCT4, SOX2 and NANOG. (C) Representative immunofluorescence labelling for the expression of neuronal stem cell markers Nestin, Sox2 and Pax6 (green or red) on Bj-iPSC-derived-NSCs. Nuclei were stained with DAPI (blue). Scale bar: 50 μm. (D) Gene expression analysis by qPCR in BJ-IPSC and NSC of NESTIN, PAX6 and SOX1. (E) Representative western blot analysis showing the time course of GFAP, EAAT1 and SOX2 protein expression during astrocyte differentiation. GAPDH was used as a loading control. (F) Growth curve of astrocytes during the differentiation process. Mean cell numbers ± standard deviations are shown. (G) Immunofluorescence labelling for the expression of GFAP in astrocytes at 30 and 56 days of differentiation. The percentage of cells displaying GFAP-positive staining is shown at the bottom of the picture. Cells in five different fields and in three independent experiments were counted blindly. The percent of GFAP-positive cells was calculated as the ratio of cells showing GFAP-positive staining compared with the total number of cells with DAPI-stained nuclei (***$P < 0.0005$, *t*-test). (H) Representative immunofluorescence double-staining images of hiPSC-derived astrocytes (at 30 days) for β3-tubulin (green)/GFAP (red), S100β (green)/GFAP (red) and EAAT1 (green)/GFAP (red). Scale bar, 100 μm. (I) Expression of the markers GFAP, S100β and EAAT1 in hiPSC-derived astrocytes as in panel G, assessed by cell count using IMAGEJ. Results from three independent experiments are reported as % of positive cells ±SEM. One-way ANOVA was performed to assess statistical significance (***$P < 0.0005$).

(Fig. 3). Although their upregulation has been reported as indicative of reactive astrocyte remodelling, elevated GFAP levels were previously attributed to *in vitro* culture conditions [19] and changes in both intermediate filament proteins and extracellular matrix proteins expression may also reflect physiological adaptive plasticity rather than being simply a reactive response to pathological stimuli [30,31]. Recently, VCAM1, BST2, ICOSL, HLA-E, PD-L1 and PDPN have been proposed as cell surface markers of reactive astrocytes [32]. Here, the proteomic analysis did not identify any of these markers of reactive astrocytes induced by proinflammatory factors (TNF, IL-1α and C1q) during hiPSC-derived astrocyte differentiation (Table S2) and did not highlight pathways strictly linked to immune response and neuroinflammation at all differentiation times. Therefore, in accordance with the literature suggesting that one or two protein markers are not sufficient to define astrocyte reactivity, but a signature of molecular markers is required [20], the proteomic data show a profile more similar to maturing astrocytes rather than to reactive ones, even at 56 days of differentiation.

Integration of proteomic and metabolomic analyses of hiPSC-derived astrocytes during differentiation

In order to obtain a detailed understanding of alterations in metabolic pathways during astrocyte differentiation, we performed metabolomic analyses and their integration with proteomic data. The shotgun label-free LC–MS/MS analyses carried out to identify major differences among samples at all the differentiation time points keeping the time 2 days as a reference, allowed to categorize the identified proteins in: (a) proteins exclusively expressed (EE) at single time points; (b) differentially expressed (DE) proteins at the selected differentiation times; and (c) proteins constantly expressed during the time course of the induced astrogliogenesis (Fig. 2C). EE and DE proteins were analysed by CLUEGO, Panther and David to find enrichments in biological processes (GOBP), molecular functions (GOMF) and pathways (Table S1G–I). Functional analysis and interpretation of proteomic profiling suggest that astrocyte differentiation induced differential expression of several proteins involved in important cellular events—e.g. glucose metabolism, aerobic metabolism and RNA metabolic processes, cytoskeleton organization, biosynthesis of various metabolites. In particular, at 15 days of differentiation proteins involved in DNA replication, synaptic vesicle trafficking, neurogenesis and immune response were more expressed (in comparison to 2 days). At 30 days proteins related to glucose metabolism, glucagon signalling and cytoskeleton organization increased, while focal adhesion and ribosome biogenesis decreased. A different picture was apparent starting from 40 days: integrin and cadherin signalling, intracellular trafficking, aerobic metabolism and RNA metabolic processes increased, whereas proteins related to the biosynthesis of various metabolites (serine, glycine, cysteine, methionine, cholesterol, pyrimidine and purine) decreased (Table S1G–I).

The metabolomic profile was determined by performing an untargeted metabolomics analysis on the same samples used for proteomic analysis. Comparing the metabolic profiles during astrogliogenesis, well-separated profiles were apparent according to partial least-squares discriminant analysis (PLS-DA), being astrocytes at 2 and 15 days of differentiation clustered closer than astrocytes at later stages (30, 40 and 56 days), and astrocytes at Day 30 being the most separated from the other groups (Fig. 4A). A number of metabolic pathways such as glycolysis, TCA cycle, PPP, amino acids and nucleotides biosynthesis, along with methionine and urea cycles, showed an overall increase of their metabolites between 15 and 30 days of differentiation, followed by a consistent decrease, which was more evident at 56 days (Table S3; Fig. 4B–E). Glutathione synthesis increased during differentiation, strongly supported by the amino acid serine (L-Ser), glutamine and glycine, which showed a maximum level at 30 days of differentiation (Fig. 5). Among the most altered amino acids was L-Ser: it reached the highest relative level at 30 days, corresponding to a 5.75-fold increase relative to Day 2, and significantly dropped afterwards at late differentiation time points. A similar trend was also observed for glycine, the alternative NMDA receptor co-agonist (Fig. 5; Table S3).

Then, proteomics and metabolomics data were integrated by METABOANALYST (Table S1L; Fig. 6). Consistent with the proliferation rate (Fig. 1F), cell-cycle functions and folate cycle increased at 15 days and then decreased after 30 days. In addition, up to 30 days the data show that axogenesis, Ala/Asp/Glu and pyrimidine metabolism were prevalent. Purine metabolism was an important point of regulation during astrogliogenesis, showing both up- and down-regulated metabolites during the time course (Fig. 6). Sphingolipid metabolism had the highest impact at 15 and 30 days, in agreement with the proliferation and maturation processes of the cells. Therefore, omics integration results pinpoint days 30 as the time of full astrocytes differentiation. Furthermore, when the omic profiles at 40 and 56 days of differentiation were

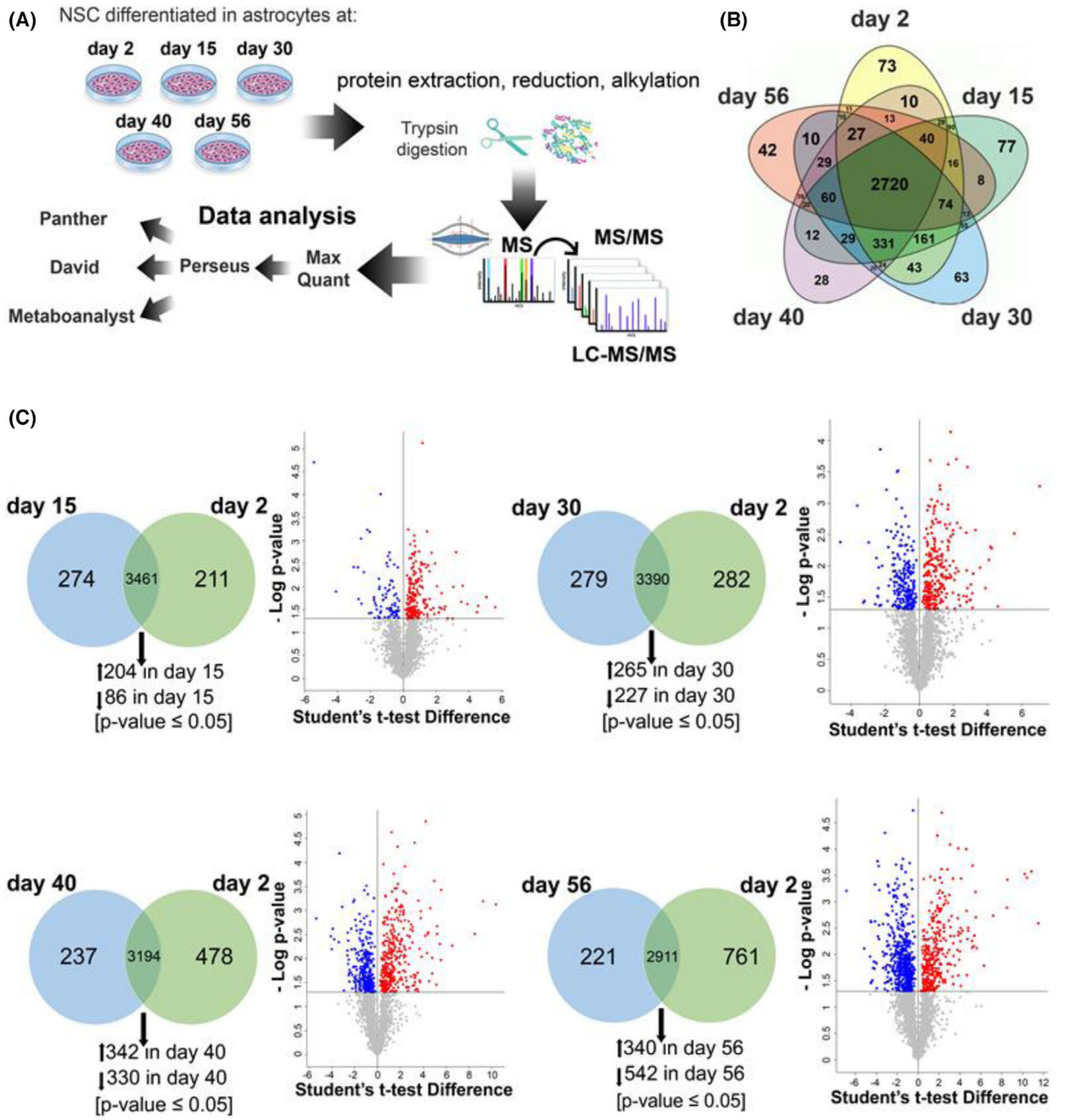

Fig. 2. Proteomic characterization of hiPSC-derived astrocytes during differentiation. (A) Overview of the protocol applied for the analysis of proteins in hiPSC-derived astrocytes. (B) Venn diagram of all the proteins identified in hiPSC-derived astrocytes at different times of differentiation. (C) Venn diagrams and Volcano plots of the comparison Day 15 vs Day 2, Day 30 vs Day 2, Day 40 vs Day 2 and Day 56 vs Day 2. Volcano plots of the DE proteins were determined using the Student's *t*-test (*P*-value 0.05). The proteins increased or decreased in each comparison are indicated in red and blue, respectively.

compared with 30 days, the integrin signalling, focal adhesion and ECM interactions were among the most enriched pathways in cells (Table S1E; Fig. 7) in line with the astrocytes maturation event that has taken place [33]. In addition, glycolysis/gluconeogenesis and ketone body metabolism were downregulated, as well as nucleotide metabolism, consistently with the arrest of proliferation from 30 to 56 days (Fig. 1F).

Concerning the energy production, ATP was mainly sustained by glucose metabolism: the rate of ATP

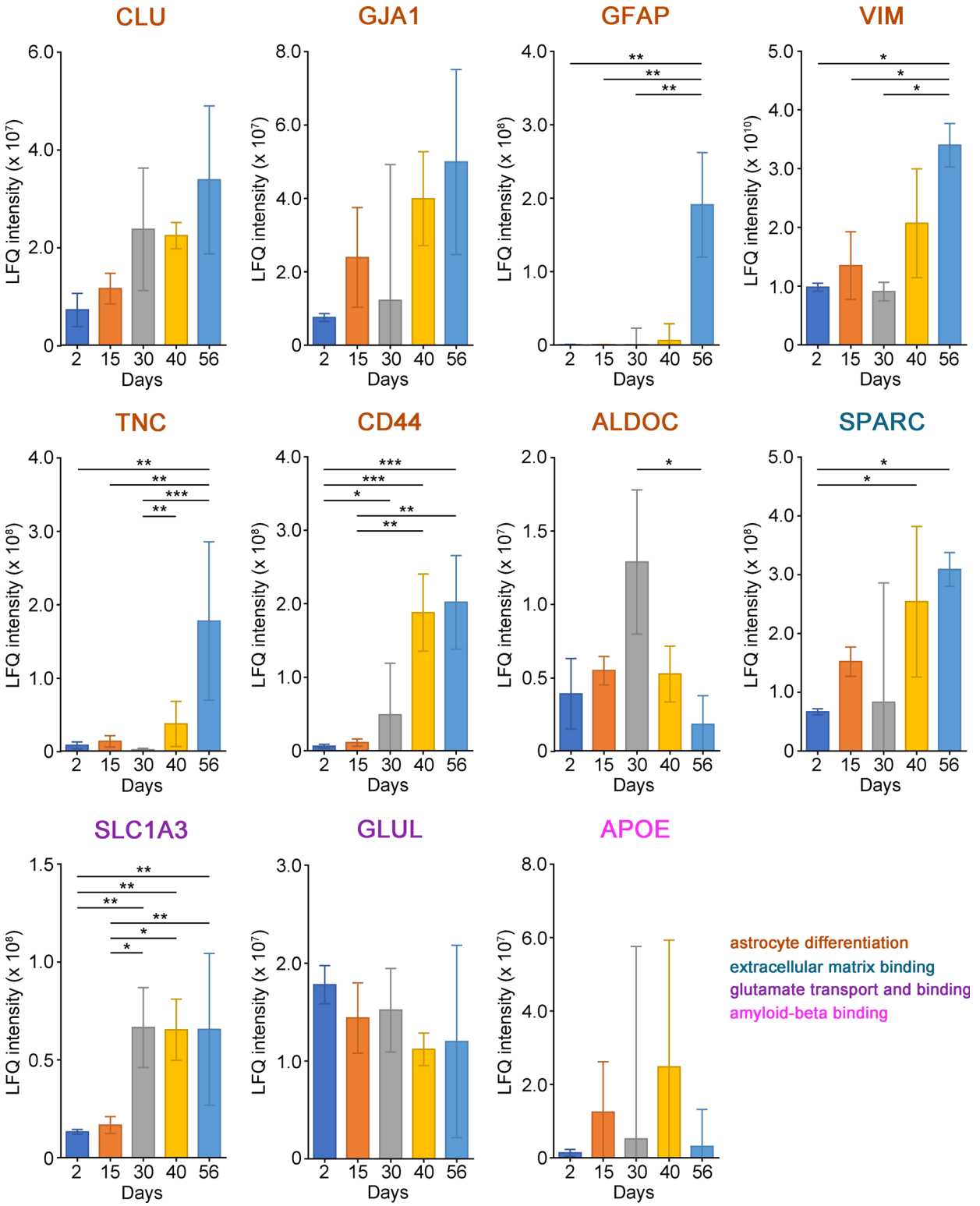

Fig. 3. Quantitative mass spectrometric analysis of the indicated markers in hiPCS-derived astrocytes. Markers are arranged by family according to the indicated colour code (astrocyte differentiation, glutamate transport and binding, extracellular matrix binding and amyloid-beta binding). Data shown are the median of LFQ intensity values obtained from 3 replicates in each group, analysed by a one-way ANOVA and Tukey's HSD *post-hoc* test (*FDR ≤ 0.05, **FDR ≤ 0.01, ***FDR ≤ 0.001).

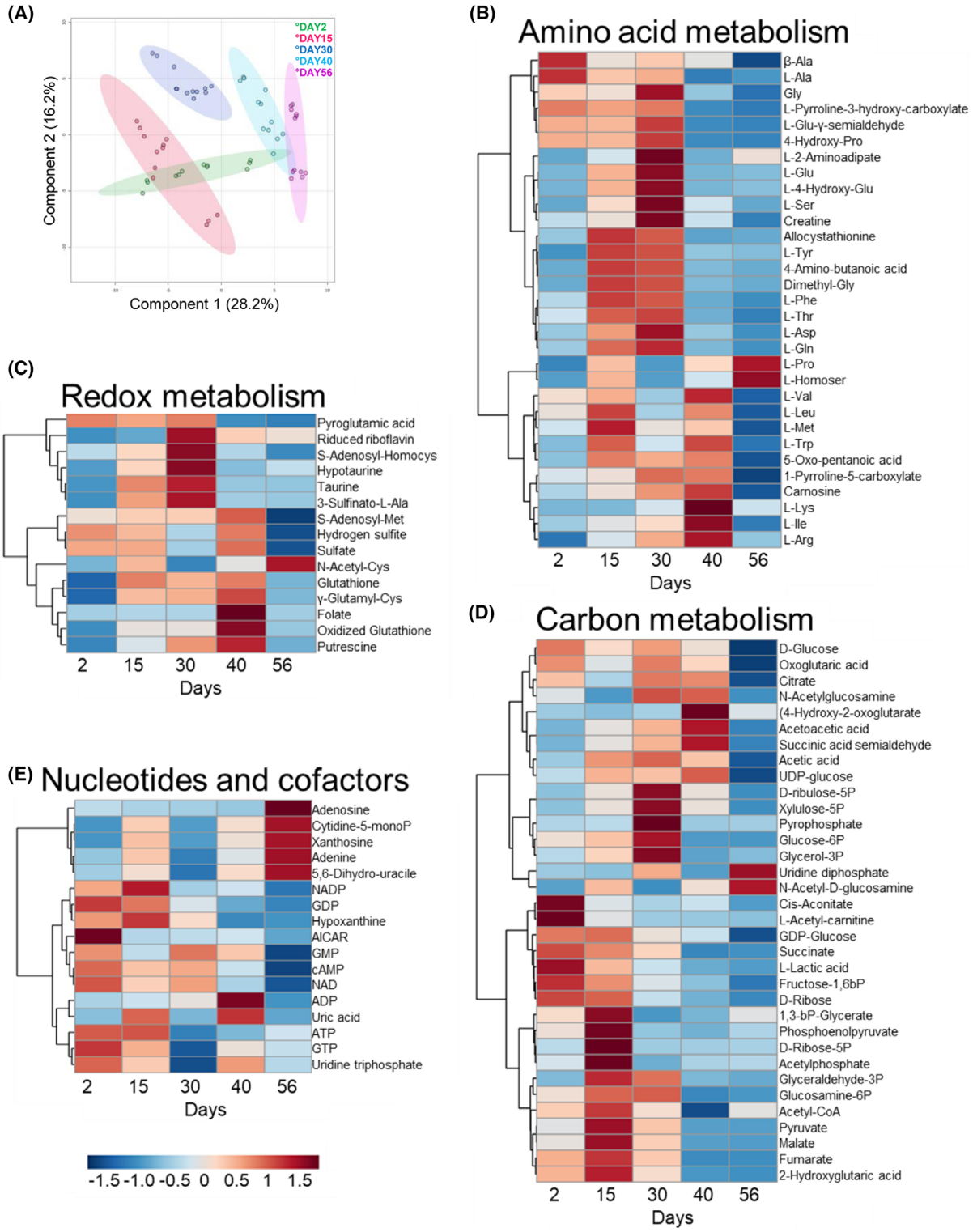

Fig. 4. Metabolomic analysis of hiPSC-derived astrocytes at different times of differentiation. (A) PLS-DA of astrocytes at 2, 15, 30, 40 and 56 days of differentiation. Analysis was performed through METABOANALYST 5.0 software. (B–E) Hierarchical clustering heatmaps from One-way ANOVA analysis of differential metabolites belonging to (B) amino acid metabolism, (C) redox metabolism, (D) central carbon metabolism, (E) nucleotides and cofactors. The heatmaps were obtained using the METABOANALYST 5.0 tool. The colour code scale indicates the normalized metabolite abundance.

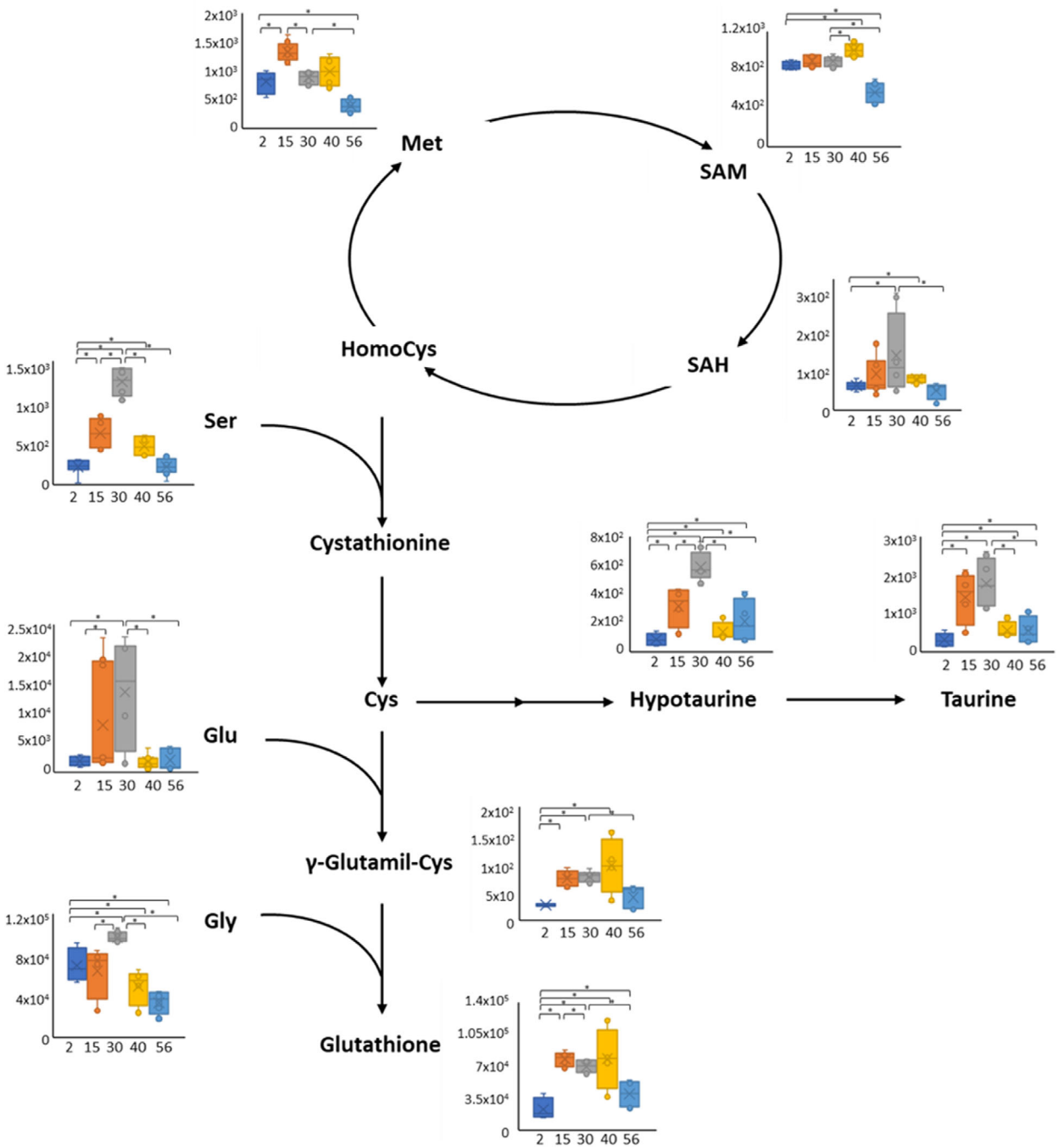

Fig. 5. Schematic representation of methionine and glutathione metabolic pathways during astrocytes differentiation. Histograms show variations of the levels of metabolites during astrocytes differentiation, detected by metabolomics analysis at 2, 15, 30, 40 and 56 days of differentiation. $*P < 0.05$ (two-tailed *t*-test).

production from glycolysis was 2.72 ± 1.06, 3.41 ± 1.05 and 3.94 ± 1.41 pmol·min^{-1}·μg^{-1} proteins at 2, 30 and 56 days, respectively (for all comparisons $P < 0.05$). Notably, the contribution of the mitochondrial activity increased during differentiation, reaching at 30 and 56 days values twice the one at 2 days (the mitochondrial ATP production rate was 0.98 ± 0.71, 1.67 ± 0.62 and 2.63 ± 0.98 pmol·min^{-1}·μg^{-1} proteins at 2, 30 and 56 days, respectively; for all comparisons $P < 0.05$).

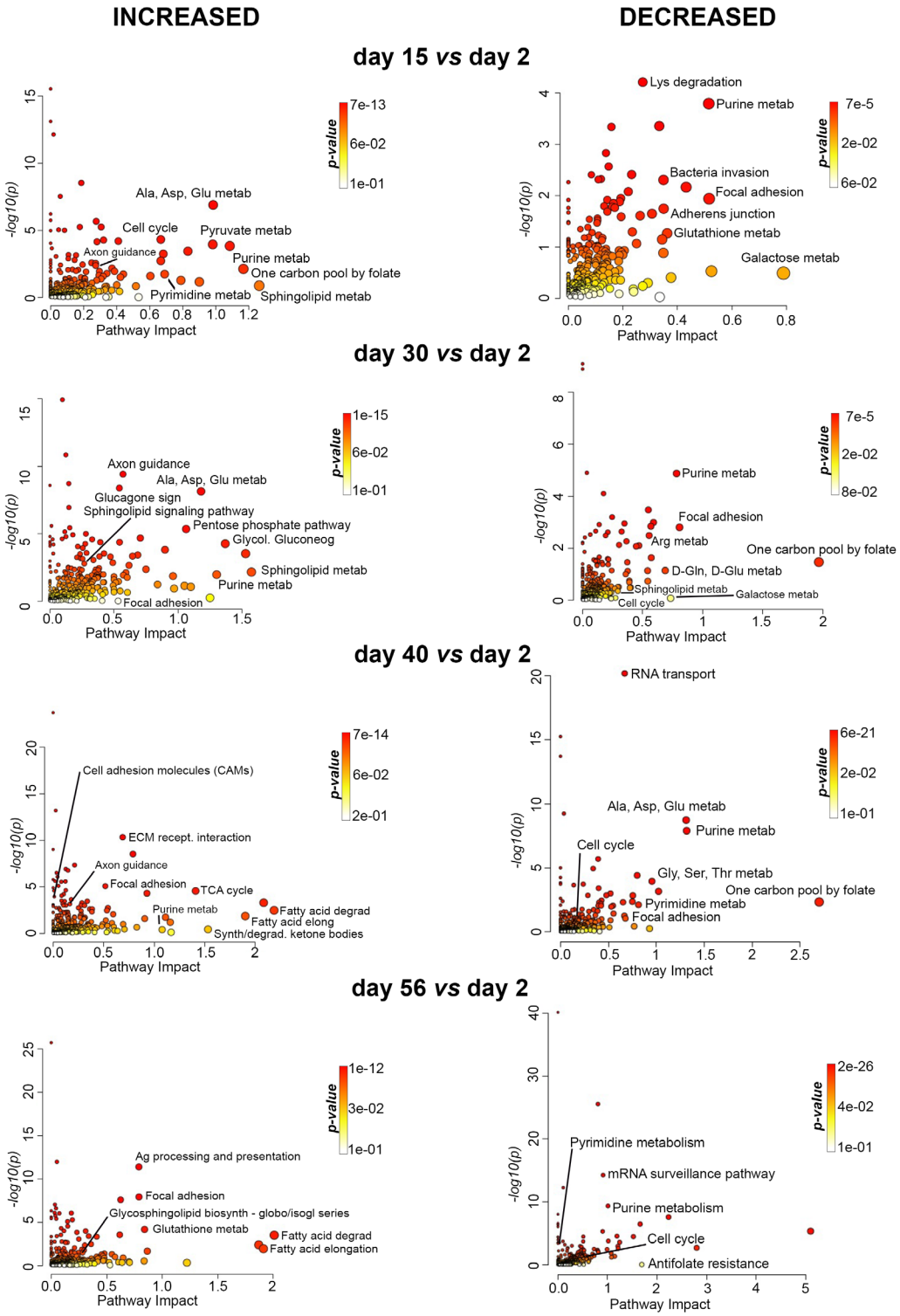

Fig. 6. Integration of proteomic and metabolomic analysis in hiPSC-derived astrocytes. Proteomic and metabolomic analyses were integrated by METABOANALYST for the proteins DE or EE in the comparison Day 15 vs Day 2, Day 30 vs Day 2, Day 40 vs Day 2 and Day 56 vs Day 2, based on a Fisher's exact test, *P*-value ≤ 0.05. Colour intensity (white-to-red) reflects increasing statistical significance, based on the *P*-value [−log *P*] from the pathway enrichment analysis, and circle dimension is based on pathway impact values from the pathway topology analysis (0–1). For clarity, only selected pathways are marked; the full list is shown in Table S1L.

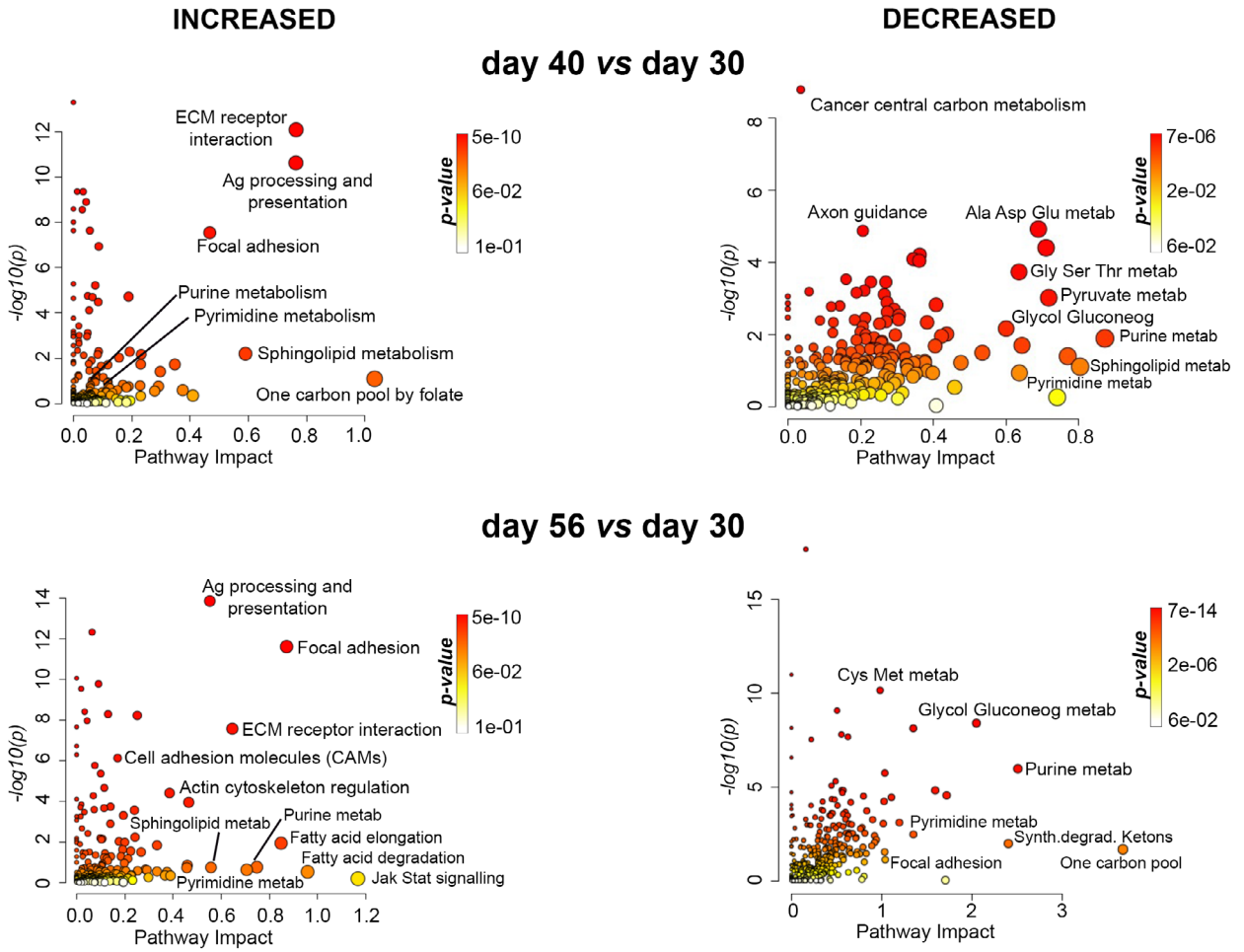

Fig. 7. Integration of proteomic and metabolomic analysis in hiPSC-derived astrocytes. Proteomic and metabolomic analyses were integrated by METABOANALYST for the proteins DE or EE in the comparison Day 40 vs Day 30 and Day 56 vs Day 30 based on a Fisher's exact test, *P*-value ≤ 0.05. Colour intensity (white-to-red) reflects increasing statistical significance, based on the *P*-value [−log *P*] from the pathway enrichment analysis and circles dimension is based on pathway impact values from the pathway topology analysis (0–1). For clarity, only few pathways are marked; the full list is shown in Table S1L.

Serine metabolism of hiPSC-derived astrocytes

Astrocytes have been increasingly recognized to play a main role in the pathophysiology of a number of degenerative diseases of the CNS [19]. An excessive stimulation of NMDA receptors is known to induce excitotoxicity in AD pathogenesis, which is due to glutamate (the agonist) and D-serine (the preferential co-agonist at the synapses) binding. Given the crucial role of astrocytes in serine biosynthesis, we focussed on enzymes and metabolites of the serine biosynthesis pathway during the time course of differentiation.

Proteomic analysis of PP enzymes and SR highlighted some differences (Fig. 8A). The expression level of PHGDH, PSAT and PSP significantly decreased at 56 days compared with 2 days of differentiation (Fig. 8A) while the expression of the enzyme SR, responsible for D-Ser production from the precursor L-Ser [34], did not show statistically significant differences during differentiation, albeit a progressive trend of increase was apparent between Days 2 and 30 (Fig. 8A, right panel). Comparison of the relative abundances of PP enzymes and SR at 30 days of differentiation showed that the latter was the less abundant, representing 0.0027 ± 0.0001% of total cellular protein content and occurring at a concentration of 0.731 ± 0.026 nmol·g^{-1} of total protein (Table S4). On the other hand, the proteins of the PP showed concentration levels from ~ 3-fold (PSP) to ~ 40-fold (PHGDH and PSAT) higher than the one for SR (Table S4).

To further confirm these data, the presence of PHGDH, PSAT, PSP, as well as D-amino acid oxidase (DAAO, the D-Ser degrading enzyme [35], which was undetectable by LC–MS/MS) and SR ones, were also analysed by western blot. No endogenous signals were detected for DAAO and SR, suggesting that their expression level was below the detection limit (0.02 and 0.04 $\mu g \cdot mg^{-1}$ total proteins, respectively). This is an interesting result for DAAO since it is mainly expressed in astrocytes in the CNS [35]. A previous study reported alterations in DNA methylation of the DAAO encoding gene in different brain regions [36]: the different methylation signatures may reflect specific functional states responsible for the flavoenzyme expression levels, a possibility that should be investigated further. On the other hand, a single relevant band was detected for PHGDH (57 kDa), PSAT (40 kDa) and PSP (30 kDa) and their concentration determined by densitometric analysis (Fig. 8B). PSP showed the lowest expression during the time course of astrocytes differentiation, ~ 10–20-fold lower than PHGDH and PSAT ones. Moreover, in keeping with proteomic data, a decreasing trend over time in the cellular levels of the enzymes of the PP was apparent, with the highest expression at 2 days and the lowest at 56 days of differentiation (Fig. 8B).

LC/MS and GC/MS analysis performed to investigate the level of metabolites related to the serine

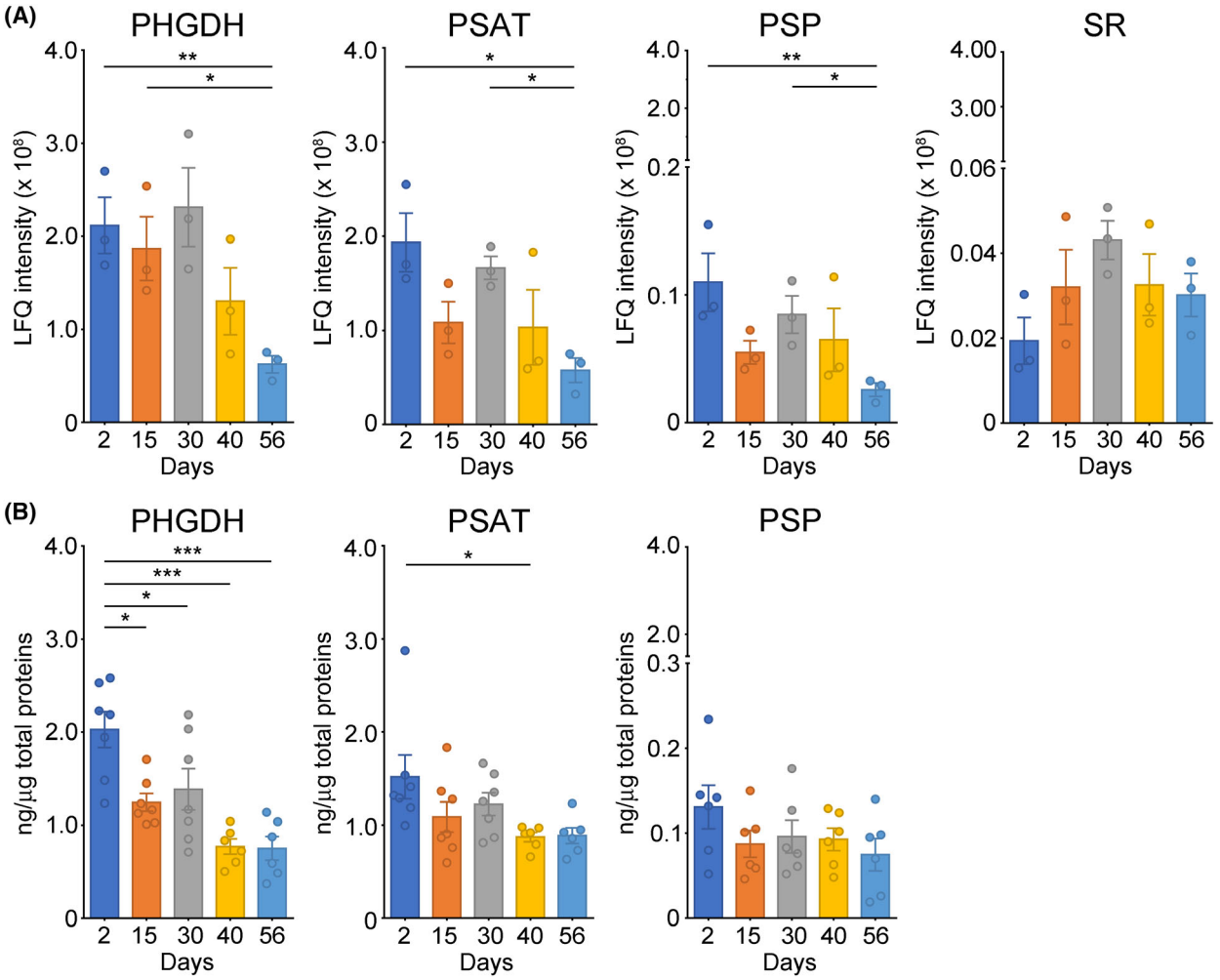

Fig. 8. PHGDH, PSAT, PSP, and SR protein levels in hiPSC-derived astrocytes during differentiation. (A) Comparison of the expression of PP's enzymes (PHGDH, PSAT, PSP) and SR in hiPCS-derived astrocytes by LC–MS/MS. The median of LFQ intensity values obtained from 3 replicates in each group was analysed by the one-way ANOVA and Tukey's HSD *post-hoc* test (*FDR ≤ 0.05, **FDR ≤ 0.01). (B) Comparison of PHGDH, PSAT and PSP levels in hiPSC-derived astrocytes determined by western blot analysis. Graphs report single data points (dots correspond to single samples). Bars represent the mean ± SEM of values obtained from 5 sets of samples; *$P < 0.05$; ***$P < 0.0005$.

biosynthetic pathway revealed that most of them showed a similar trend, with a maximum at 30 days of differentiation and a strong decrease at 40 and 56 days (Fig. 9), when the PP enzymes levels showed the most significant decrease (Fig. 8). This was the case of serine itself, glycine, threonine and aspartate but also of glutamine and glutamate, which is the amino donor in the second step of the PP: the ensuing α-keto-glutarate product could then be used in the TCA cycle. Strikingly, most metabolites of the TCA cycle showed a decrease at 40 and 56 days of differentiation, similarly to those of the serine pathway (Fig. 9).

To discriminate between the L- and the D-enantiomers, chiral high-performance liquid chromatography (HPLC) analysis was performed. The analyses revealed a statistically significant increase in L-Ser, D-Asp and L-Asp levels during cell differentiation, with a peak at 30 days and a slow decrease afterwards (Fig. 10A). This tendency, which is in accordance with metabolomic data (Fig. 9), was also observed for D-Ser and Gly, although in these cases no statistical significance at 30 days compared with 2 days of differentiation was evident. Intriguingly, the trend of D-Ser level paralleled the SR protein level (Fig. 8A). The relative levels of D-Ser and D-Asp detected in differentiated astrocytes were significantly different from those previously reported in various cell lines: at 30 days of differentiation D-Ser content was up to 5-fold lower than in human neuroblastoma SH-SY5Y cells and in human glioblastoma U87 cells [37], whereas D-Asp levels were very high. Conversely, L-Ser and L-Asp content in differentiated astrocytes and cell lines appeared similar [37]. Consequently, the D-/(D + L)-amino acid ratio was also significantly different: this value decreased in differentiated astrocytes vs neuroblastoma SH-SY5Y and glioblastoma U87 cells for serine (0.8% vs 1.24% and 1.46%, respectively) and increased for aspartate (3.45% vs 1.08% and 0.58%, respectively).

Measurements of key metabolites in the conditioned culture media (recovered after 2 days of growth at the indicated times and compared with the values determined in the unconditioned medium) showed a significant increase in their level for L-Asn, which was apparent especially at 2 days, and for L-Asp and L-Glu, with a maximum between 15 and 30 days (Fig. 10B). The release of L-Glu in the culture medium seems not related to Best1 transporter (suggested to release D-Ser too) [38] since its level was below detection in MS analysis at all differentiation times. Focussing on additional aspartate/glutamate transporters [39], proteomics analysis identified many of them during the whole differentiation, but the differences in their expression level were not statistically significant with the only exception for SLC1A3, a symporter primarily expressed in the cerebellum and cerebral cortex, whose level presented a significant increase at 30 days compared with 2 days (Fig. 11) in keeping with the increase of L-Glu level in the culture medium at 30 days. Coherently, the maximum consumption of L-Gln from the medium was at 30 days too (Fig. 10B), the proteomics analysis suggests that the influx of L-Gln could be mediated by SLC38A2 transporter (Fig. 11). Concerning amino acid consumption from the medium, a huge utilization of L-Ser was apparent at all times, especially at 2 days, while small alterations were observed in D-Ser level (Fig. 10B). Proteomic analysis suggests that cellular uptake and release of serine in astrocytes could be mediated by SLC1A5 transporter [40], an antiporter whose expression level was high at 2 and 15 days and significantly decreased from 30 days (Fig. 11). Compared with the levels detected in the unconditioned medium, Gly was consumed at 2 days and then released in the medium, with a peak at 30 days (Fig. 10B), a behaviour parallel to the intracellular Gly level, which was high until Day 30 (Fig. 9). Finally, in keeping with the astrocyte neuron lactate shuttle hypothesis [24], a continuous lactate secretion in the media was evident starting from Day 2 (Fig. 10B), while intracellular lactate strongly decreased during astrocytes differentiation (Fig. 4D). In accordance, proteomics data suggest a constant expression level of MCT1 transporter (which regulates lactate fluxes) [41] (Fig. 11D), with no statistical differences during the differentiation process.

Discussion

Neural stem cells are multipotent cells present in the developing brain: they continue to produce the three neural lineages (i.e. neurons, astrocytes and oligodendrocytes) in adult brains [3]. Astrocytes, the most abundant cells in the brain, play crucial roles in the CNS such as energy metabolism, ionic homeostasis and synaptic transmission. On this side, glutamatergic and GABAergic neurotransmission processes depend on astrocytic metabolism for neurotransmitter replenishment [42]. Moreover, astrocytes have been suggested as contributors to neurodegenerative disorders by various mechanisms, including metabolic alterations [43].

In this work, we present a multi-omics analysis during the specification of astrocytes from NSCs. A hiPSC line from human fibroblasts was differentiated into NCS using the GIBCO protocol: NSC colonies expressed typical markers, including Nestin, SOX1, Sox2 and Pax6 (Fig. 1C,D). A monolayer protocol

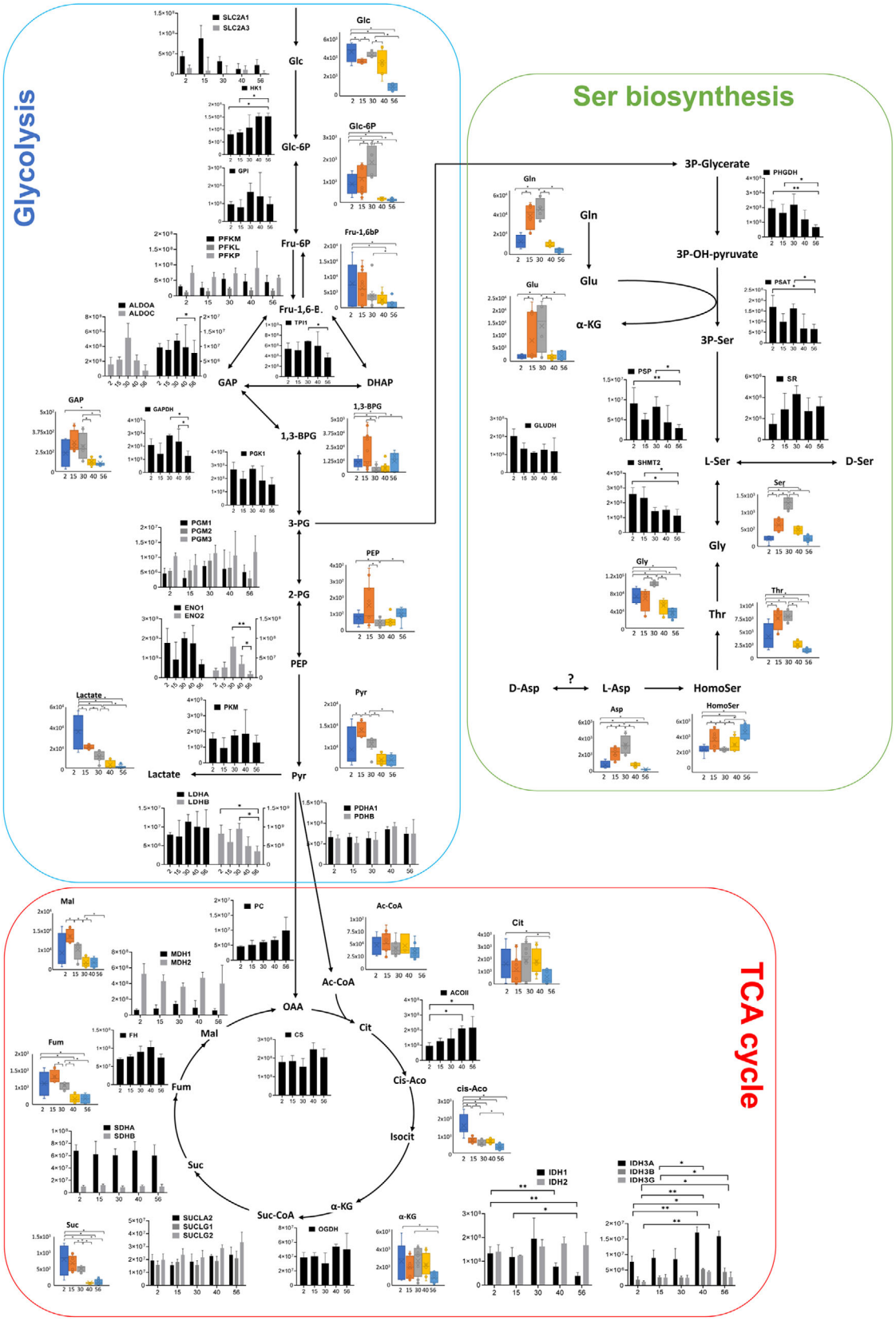

Fig. 9. Serine metabolism and related pathways in hiPSC-derived astrocytes. Schematic representation of serine biosynthesis (green box) and related main pathways (TCA cycle in red box and glycolysis in blue box). Histograms show variations of the levels of metabolites and enzymes during differentiation at 2, 15, 30, 40 and 56 days, detected by metabolomic and proteomic analysis. $*P < 0.05$. Values of fold changes and *t*-test from metabolomic analysis are reported in Table S3. Proteomic data shown are the median of LFQ intensity values obtained from 3 replicates in each group analysed by a one-way ANOVA and Tukey's HSD *post-hoc* test (*FDR ≤ 0.05, **FDR ≤ 0.01). The proteins are indicated by the official gene code. ACOII, aconitate hydratase; ALDOA, fructose-bisphosphate aldolase A; ALDOC, fructose-bisphosphate aldolase C; CS, citrate synthase; ENO1, alpha-enolase; ENO2, gamma-enolase; FH, fumarate hydratase; GAPDH, glyceraldehyde-3-phosphate dehydrogenase; GLUDH, glutamate dehydrogenase; GPI, glucose-6-phosphate isomerase; HK1, hexokinase-1; IDH1, isocitrate dehydrogenase (NADP) cytoplasmic; IDH2, isocitrate dehydrogenase (NADP), mitochondrial; IDH3A, IDH3B, IDH3G, isocitrate dehydrogenase (NAD) subunit alpha, beta and gamma; LDHA, L-lactate dehydrogenase A chain; LDHB, L-lactate dehydrogenase B chain; MDH1, malate dehydrogenase, cytoplasmic; MDH2, malate dehydrogenase, mitochondrial; OGDH, 2-oxoglutarate dehydrogenase; PC, pyruvate carboxylase; PDHA1, pyruvate dehydrogenase E1 component subunit alpha; PDHB, pyruvate dehydrogenase E1 component subunit beta; PFKL, ATP-dependent 6-phosphofructokinase, liver type; PFKM, ATP-dependent 6-phosphofructokinase, muscle type; PFKP, ATP-dependent 6-phosphofructokinase, platelet type; PGK1, phosphoglycerate kinase 1; PGM1, PGM2, PGM3, phosphoglucomutase-1-3; PHGDH, D-3-phosphoglycerate dehydrogenase; PKM, pyruvate kinase; PSAT, phosphoserine aminotransferase; PSP, phosphoserine phosphatase; SDHA, succinate dehydrogenase (ubiquinone) flavoprotein subunit; SDHB, succinate dehydrogenase (ubiquinone) iron–sulfur subunit; SHMT2, serine hydroxymethyltransferase; SLC2A1, solute carrier family 2, facilitated glucose transporter member 1; SLC2A3, solute carrier family 2, facilitated glucose transporter member 3; SR, serine racemase; SUCLA2, succinate-CoA ligase (ADP-forming) subunit beta; SUCLG1, succinate-CoA ligase (ADP-forming) subunit alpha; SUCLG2, succinate-CoA ligase (GDP-forming) subunit beta; TPI1, triosephosphate isomerase.

was then used to differentiate NSCs into astrocytes: based on classical astrocytes markers (GFAP and EAAT1, that reached the highest level between 30 and 56 days) and markers of NSC (which progressively downregulated over time), we concluded that at 30 days mature astrocytes were generated (all cells were $S100\beta^+$ and $EAAT1^+$, with a high proportion of $GFAP^+$ cells); the neuronal marker β3 tubulin was undetectable at Day 30 (Fig. 1H) thus excluding any contamination of neurons. Despite the increase of GFAP, tenascin and vimentin proteins expression detected at 56 days of differentiation (Fig. 3), all the other markers of activated astrocytes described in the literature were absent or not statistically different suggesting a pattern of maturing astrocytes rather than cells in a reactive state even at 56 days of differentiation.

A previous work reported significant metabolic differences between mouse NSCs and astrocytes, with a general downregulation of central carbon metabolism during astrocytic differentiation [24]. In detail, while a high lactate-secreting phenotype was common to both cell types, glucose uptake was 1.7-fold higher in NSCs, which also consumed glutamine from the medium (converted to citrate and used for biosynthetic purposes). Concerning cytosolic pyruvate, most of it was diverted to lactate secretion in astrocytes (in good agreement with the observed high extracellular lactate, and the high expression level of MCT1 transporter observed in our experiments, see Figs 9 and 11) while half was converted to mitochondrial pyruvate in NSCs. In astrocytes, the metabolism of mitochondrial pyruvate was largely through pyruvate carboxylase, an anaplerotic metabolization of pyruvate that contributed to support glutamine and citrate secretion. The extracellular levels of L-Glu and L-Asp significantly increased, reaching a maximum at 30 days (Fig. 10): MS analysis highlights substantial differences of SLC1A3 transporter (suggested to regulate cell glutamate efflux in tumour microenvironment) with a significant increase at 30 days compared with 2 days (Fig. 11). When NCS proliferated and differentiated into neurons, D-Ser was produced and released while extracellular L-Glu level was unchanged [44]. Notably, our results show an opposite behaviour, with a strong L-Glu release in the medium starting from 15 days (coherent with the maturation of astrocytes) and no statistically significant change in extracellular D-Ser level (Fig. 10B).

Concerning the metabolism of L-Ser, a decrease in the level of the enzymes of the PP during differentiation of NCS in astrocytes was apparent, reaching a steady level at times ≥ 15 days (Fig. 8). The levels of cellular total serine increased up to 30 days, with a moderate increase in D-Ser ones, which parallels the levels of the synthetic enzyme SR (Fig. 8). The downregulation of the PP enzymes might probably be ascribed to the ability of the cells to use L-Ser largely present in the medium (0.24 mM), a condition that might repress its endogenous synthesis. By evaluating cellular levels and the most altered metabolic pathways, it seems that intracellular L-Ser could be diverted to glutathione synthesis until 30 days of differentiation, as well as for glycine, with minimal D-Ser

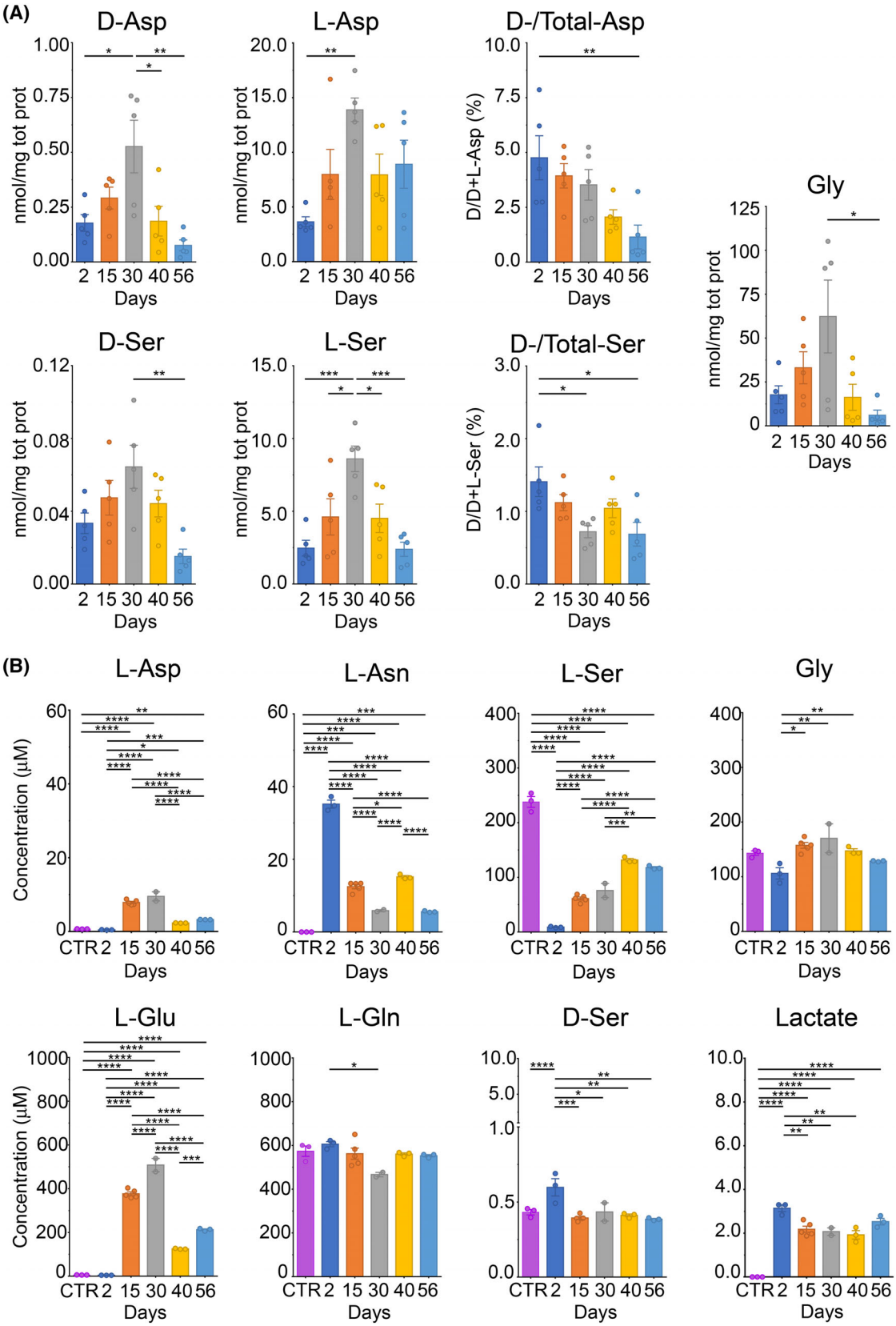

Fig. 10. Level of intracellular and extracellular selected amino acids and lactate during astrocytes differentiation. (A) D- and L-Asp, D- and L-Ser, Gly levels and ratio between D-/total-amino acid content (for Asp and Ser) detected in hiPSC-derived astrocytes at different times of differentiation by HPLC analysis. Graphs report single data points (corresponding to single biological replicates analysed in 3 technical replicates) as well as mean values ± SEM. (B) Concentrations of L-Asp, L-Asn, L-Glu, L-Gln, Gly, L-Ser, D-Ser and lactate were determined in the medium of astrocytes at different times of differentiation. Media were collected after 2 days of growth at the indicated times of differentiation. Graphs report single data points (corresponding to single biological replicates analysed in three technical replicates), as well as mean values ± SEM, analysed by a one-way ANOVA multiple comparison. $*P < 0.05$, $**P < 0.01$, $***P < 0.001$, $****P < 0.0001$.

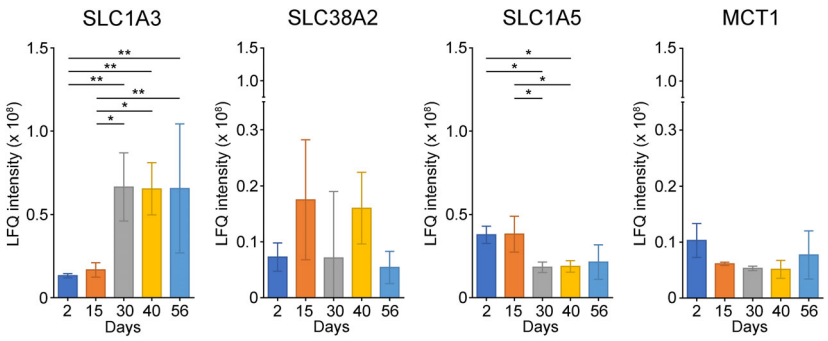

Fig. 11. Quantitative mass spectrometric analysis in astrocytes during differentiation of selected transporters: aspartate/glutamate transporter SLC1A3, glutamine transporter SLC38A2, serine transporter SLC1A5 and lactate transporter MCT1. Data shown are the median of LFQ intensity values obtained from 3 replicates in each group analysed by a one-way ANOVA and Tukey's HSD *post-hoc* test (*FDR ≤ 0.05, **FDR ≤ 0.01). Undetectable: SLC1A1, SLC1A2, SLC1A6, SLC17A7, SLC1A4, SLC7A10, SLC38A5, SLC16A3, SLC5A8 and SLC5A12.

production (as suggested by the observed decrease in D-/total serine ratio during differentiation, Fig. 10A). Actually, a true competition with D-Ser synthesis was not apparent since the detected levels of D-Ser were low as compared to other cell lines—e.g. the level of D-Ser was 0.34 nmol·mg^{-1} protein in human neuroblastoma SH-SY5Y cells or 0.12 nmol·mg^{-1} proteins in glioblastoma U87 cells [37]. Furthermore, the level of D-Ser in differentiated astrocytes was 10-fold lower compared with D-Asp level (normally D-Asp is present at very low concentrations, significantly below D-Ser ones) [45,46]. The ability of differentiated astrocytes to produce D-Asp is a point that deserves additional investigations since the origin of this D-amino acid is still debated—the presence of a specific racemase is still questioned [47,48]. Notably, Baier *et al.* [49] showed that cultured mouse astrocytes produce SR in low amount early in culture (but its actual level was not quantified), a figure that increased significantly in 7 days (~ 3-fold) with an increase in D-Ser level in the culture medium and with the expression of markers of A1 reactive astrocytes (e.g., Complement 3a). Based on the analysis of selected markers, we conclude that human astrocytes differentiated from NCS by the Gibco protocol did not convert into A1 reactive astrocytes and, thus, did not express SR to a significant level: this prevents a significant D-Ser production.

L-Ser synthesis is also related to the main energetic metabolism. The level of glucose-6-phosphate increased until 30 days of differentiation when the maximal level of ATP was also observed: at this time point the level of ATP arising from glycolysis was increasing (Fig. 7B), suggesting that from this moment glucose-6-phosphate was of main relevance for energy generation. Notably, also the glucose level decreased after 30 days of differentiation and this reduced the stabilization of PHGDH: actually, glucose controls acetylation of K58 in PHGDH, protecting the dehydrogenase from degradation through RNF5 E3 ubiquitin ligase. A decrease in glucose was previously reported to induce a decrease in serine and glycine level, ROS increase and cell growth inhibition [50]. These latter observations suggest that 30 days represent a switch for the terminal differentiation and the set-up of the physiological metabolic profile of differentiated astrocytes (as we observed at ≥ 40 days).

In conclusion, the proliferation and differentiation of NSCs play a crucial role to ensure neurogenesis and gliogenesis in the mammalian brain throughout life. As there is growing evidence for the significance of metabolism in regulating cell fate, knowledge on the metabolic programmes in NSCs and how they change during differentiation into somatic cells may provide novel therapeutic approaches to address brain diseases,

especially the ones related to serine metabolism alterations.

Materials and methods

Cells

Human fibroblasts from ATCC [BJ (ATCC CRL-2522, Manassas, VA, USA)] were reprogrammed into hiPSC utilizing SENDAI virus carrying the embryonic genes OCT4, SOX2, KLF4 and cMYC, under defined-media conditions completely free of non-human, animal materials. Colonies were mechanically picked between Days 20 and 25. hiPSC cultures were monitored every day. Prior to manual isolation, colony boundaries may be difficult to visualize due to the high-density nature of the culture at this stage in reprogramming. The use of live-staining antibodies (mouse anti-human TRA-1-60 or TRA-1-81) enabled rapid identification of reprogrammed clones prior to colony picking and expansion. At least three hiPSC clones were expanded. Once identified hiPSC lines on the basis of their ES (embryonic stem)-like morphology, molecular analyses were carried out to verify their pluripotency: (a) immunostaining for the expression of OCT4, SSEA4; (b) qRT-PCR for the expression of the pluripotency-associated transcripts OCT, SOX2 and NANOG.

Differentiation of hiPSCs into NSCs

High-quality hiPSCs were cultured in feeder-free conditions in Essential 8 Medium on Geltrex substrate. When the hiPSCs reached ~ 70–80% confluency, the cells were dislodged into a single-cell suspension and plated at 3×10^4 cells·cm^{-2}. After 24 h the medium was changed from Essential 8 to PSC Neural Induction Medium (A1647801; Thermo Fisher, Waltham, MA, USA). The medium was changed every 2 days and any non-neural differentiated cells were removed. On Day 7 of neural induction, cells reached confluency and were ready to be harvested and expanded. Cells were dissociated, gently pipetted up and down to break up the cell clumps and plated on Geltrex at a density of 5×10^4 cells·cm^{-2} in Neural Expansion Medium composed of PSC Neural Induction Medium and Advanced DMEM/F-12 Medium (12634; Thermo Fisher) at 1 : 1 ratio. Neural Expansion Medium was exchanged every other day thereafter. NSCs reached confluency on Days 4–6 after plating, then were characterized, expanded, cryopreserved or differentiated into astrocytes.

Neural stem cells were differentiated in astrocytes by seeding dissociated single cells at 25 000 cells·cm^{-2} density on Geltrex (12760; Thermo Fisher)-coated plates in astrocytes medium composed of DMEM 1× (11995; Thermo Fisher), 1% fetal bovine serum ES qualified (16141; Thermo Fisher), 2 mM Glutamax (35050; Thermo Fisher), 1% N2 supplement (17502; Thermo Fisher) and 1× antibiotic antimycotic solution (15240; Thermo Fisher). The medium was replaced with fresh medium every 3–4 days. When the cells reached 90–95% confluency (approximately every 4–5 days), they were split to the initial seeding density (25 000 cells·cm^{-2}) as single cells in astrocyte medium and cultured on Geltrex, following 5–10 min incubation with accutase (A1110501; Thermo Fisher), pipetting and washing with DMEM. Cells were collected during the differentiation process at Days 2, 15, 30, 40 and 56 for multi-omics analysis.

Immunofluorescence

Cells were plated on Geltrex-precoated coverslips at 2×10^4 cm^{-2} on a 24-well plate. Within 24 h, NSC and astrocyte cultures were washed with PBS and fixed using 4% paraformaldehyde (Sigma-Aldrich, St. Louis, MI, USA) for 20 min, washed three times with PBS 1×, permeabilized in PBS1 × – 0.2% Triton X-100 for 15 min at room temperature (RT) and then incubated with blocking solution made of PBS 1× (0.2% Triton X-100, 10% donkey serum; Jackson ImmunoResearch, WestGrove, PE, USA), for at least 1 h. Cultures were then incubated with the primary antibody diluted in blocking solution, overnight at 4 °C, followed by incubation with the secondary antibodies for 1 h at RT. Primary antibodies used in this study were S100β (mouse, 1 : 1000, S2532; Sigma-Aldrich), GFAP (Rabbit, 1 : 300; Dako, Santa Clara, CA, USA), Vimentin (rabbit, 1 : 500, R28#3932; Cell Signalling, Danvers, MA, USA), β-III-tubulin (rabbit, 1 : 1000, 802001; Biolegend, San Diego, CA, USA), GLAST/EAAT1 (mouse, 1 : 100; Santa Cruz Biotechnologies, Dallas, TX, USA); Nestin (mouse 1 : 100 USAMAB353; 1 : 100; Chemicon International, Temecula, CA, USA); Sox2 [1 : 200 rabbit monoclonal (EPR3131; ab92494) Abcam, Cambridge, UK]; Sox2 (goat 1 : 150; Santa Cruz Biotechnologies); Pax6 (rabbit 1 : 200; Pluripotent Stem Cell Immunocytochemistry Kit; OCT4, SSEA4; A25526; ThermoFisher).

Secondary antibodies used were Alexa Fluor 488, 568 or 647 conjugated (1 : 300; Jackson ImmunoResearch). Cultures were counterstained using 4′,6-diamidino-2-phenylindole (DAPI, 1 : 1000, D1306; Invitrogen, Whaltman, MA, USA). Prolong antifade gold mounting solution (P10144; Invitrogen) was used to mount on coverslips. Images were obtained by laser scanning confocal microscopy using a TCS-SP5 microscope (Leica Microsystems GmbH, Wetzlar, Germany). All analyses were performed in sequential scanning mode to rule out cross-bleeding between channels.

Microscope, images acquisition and quantification

Fluorescence images were acquired on a TCS-SP5 confocal laser scanning microscope (Leica Microsystems GmbH) using 40 × 1.35 NA oil immersion objective. High-

resolution images were acquired as z-stack with a 0.5 μm z-interval (at least 10 planes) and converted to maximum projection images (to avoid subjectivity in the choice of the plane to be analysed) with the LASAF software platform (Leica Microsystem) in the TIFF format.

Quantification of the number of astrocytes positive for GFAP, S100β and GAST1 was performed using IMAGEJ (NIH, Bethesda, MD, USA) according to IMAGEJ guidelines for automatic cell counting. In the different figures, each bar (mean ± SEM) represents the mean obtained from the quantification of signals from 10 different fields from three independent experiments.

Western blot

Human induced pluripotent stem cells-derived astrocytes (5 sets of samples) at different times of differentiation (2, 15, 30, 40 and 56 days) were homogenized in 0.1 mL of 0.2 M TCA (trichloroacetic acid), sonicated (three cycles, 10 s each) and then centrifuged at 13 000 ***g*** for 20 min. The supernatants were stored at −80 °C for HPLC analysis. The pellets were solubilized in 1% SDS, sonicated (three cycles, 10 s each) and then centrifuged at 13 000 ***g*** for 20 min. The protein concentration in the supernatants was quantified using the Bradford reagent (500-0205; BioRad, Segrate, Italy). These samples were analysed by western blot for the presence of PHGDH (rabbit anti-PHGDH, HPA024031; Sigma-Aldrich, dilution 1 : 1000), PSAT (rabbit anti-PSAT, abin2856767; Antibodies online, Pottstown, PA, USA, 1 : 1000), PSP (rabbit anti-PSP, PA5-22003; Invitrogen, dilution 1 : 1000), DAAO (rabbit anti-hDAAO, ab187525; AbCam, 1 : 2000), SR (rabbit anti-SR; Davids Biotechnologie, Regensburg, Germany, home-made, 1 : 100). For each sample 20 μg (for PHGDH, PSAT and PSP) or 40 μg (for DAAO and SR) of total proteins were separated by SDS/PAGE and then transferred on a PVDF membrane using the Mini Trans-Blot Cell system (BioRad). The membrane was blocked overnight at 4 °C with 4% dried milk in Tris-saline buffer pH 8.0 added of 0.1% Tween20 and subsequently incubated with primary antibodies diluted in 2% dried milk in Tris-saline buffer pH 8.0 added of 0.05% Tween20 for 2 h at RT. After extensive washings, the membrane was incubated for 1 h at RT with anti-rabbit IgG (Alexa Fluor Plus 800, 1 : 20 000 dilution in Tris-saline buffer pH 8.0 added of 0.05% Tween 20). Membranes were analysed by Li-cor IMAGESTUDIO software (Li-Cor Biosciences, Lincoln, NE, USA): the intensity signal of each sample was normalized by the GAPDH signal (detected using a mouse anti-GAPDH, 1 : 2000, MA5-15738 Invitrogen and a mouse IgG IRDye 680 1 : 5000). The content of each protein was calculated by the software based on the intensity of known amounts of recombinant proteins and was related to the mg of total proteins loaded into the gel. Controls included the addition of a known amount of each recombinant protein to the samples (10 ng for PHGDH, PSAT, DAAO and SR; 1 ng for PSP). Each sample was analysed at least three times (in three different SDS/PAGE runs). The results were analysed using PRISM (Graphpad Software Inc., San Diego, CA, USA). Variation of protein levels between different times of differentiation was evaluated using the one-way ANOVA, Tukey's test. A P-value < 0.05 was considered as statistically significant.

Growth curves

Cells were seeded at 25 000 cells·cm^{-2} density on Geltrex-coated plates and differentiated as described above. When the cells reached 90–95% confluency, they were counted and splitted to the initial seeding density (25 000 cells·cm^{-2}) as single cells in astrocyte medium. Growth curves are presented in a semi-log scale.

Chemicals for metabolomics analysis

All chemicals and solvents used for extraction buffer and for liquid chromatography were LC–MS Chromasolv purity grade. Acetonitrile, methanol, 2-propanol and water were purchased from Honeywell, while chloroform and formic acid were purchased from Sigma-Aldrich.

GC–MS metabolic profiling

GC–MS metabolic profiling was conducted essentially as in Ref. [51]. Cells were quickly rinsed with 0.9% NaCl and quenched with 800 μL of 1 : 1 ice-cold methanol : water and collected by scraping. Cells were sonicated 5 s for 5 pulses at 70% power twice, and then, 400 μL of chloroform was added. Samples were vortexed at 4 °C for 20 min and then centrifuged at 12 000 ***g*** for 10 min at 4 °C. The aqueous phase was collected in a glass insert for solvent evaporation in a centrifugal vacuum concentrator (Concentrator plus/Vacufuge® plus; Eppendorf, Hamburg, Germany) at 30 °C for about 2.5 h.

Derivatization was performed using an automated sample preparation WorkBench instrument (Agilent Technologies, Santa Clara, CA, USA). Dried polar metabolites were dissolved in 60 μL of 2% methoxyamine hydrochloride in pyridine (Thermo Fisher) and held at 40 °C for 6 h. After the reaction, 90 μL of MSTFA (*N*-methyl-*N*-(trimethylsilyl) trifluoroacetamide) was added, and samples were incubated at 60 °C for 1 h. Derivatized samples were analysed by GC–MS using a DB-35MS column (30 m × 0.25 mm i.d. × 0.25 μm) installed in an Agilent 7890B gas chromatograph interfaced with an Agilent 7200 Accurate-Mass Quadrupole Time-of-Flight (QTOF) mass spectrometer, operating under electron impact (EI) ionization at 70 eV. Samples (1 μL) were injected in a splitless mode at 250 °C, using helium as the carrier gas at a flow rate of 1 mL·min^{-1}. The GC oven temperature was held at 100 °C for 2 min and increased to 325 °C at 10 °C·min^{-1}. GC/MS

data processing was performed using Agilent MASS HUNTER software. Relative metabolites abundance was carried out after normalization to internal standard d27 Myristic acid and cell number and statistical analyses were performed using METABOANALYST 5.0 [52].

LC–MS metabolic profiling

LC–MS metabolic profiling was conducted essentially as in Ref. [51]. Cells were quickly rinsed with 0.9% NaCl and quenched with 500 µL ice-cold 70 : 30 acetonitrile water. Plates were placed at −80 °C for 10 min, then the cells were collected by scraping. Cells were sonicated as above and then centrifuged at 12 000 ***g*** for 10 min at 4 °C. The supernatant was collected in a glass insert and dried as above. Samples were then resuspended with 150 µL of H_2O prior to analyses.

LC separation was performed using an Agilent 1290 Infinity UHPLC system and an InfinityLab Poroshell 120 PFP column (2.1 × 100 mm, 2.7 µm; Agilent Technologies). Mobile phase A was water with 0.1% formic acid. Mobile phase B was acetonitrile with 0.1% formic acid. The injection volume was 15 µL and LC gradient conditions were: 0 min: 100% A; 2 min: 100% A; 4 min: 99% A; 10 min: 98% A; 11 min: 70% A; 15 min: 70% A; 16 min: 100% A with 5 min of post-run. Flow rate was 0.2 $mL{\cdot}min^{-1}$, and the column temperature was 35 °C. MS detection was performed using an Agilent 6550 iFunnel QTOF mass spectrometer with Dual JetStream source operating in negative ionization mode. MS parameters were: gas temperature: 285 °C; gas flow: 14 $L{\cdot}min^{-1}$; nebulizer pressure: 45 psig; sheath gas temperature: 330 °C; sheath gas flow: 12 $L{\cdot}min^{-1}$; VCap: 3700 V; Fragmentor: 175 V; Skimmer: 65 V; Octopole RF: 750 V. Active reference mass correction was through a second nebulizer using masses with *m*/*z*: 112.9855 and 1033.9881 dissolved in the mobile phase 2-propanol-acetonitrile-water (70 : 20 : 10 v/v). Data were acquired from *m*/*z* 60–1050. Data analysis and isotopic natural abundance correction were performed with MASSHUNTER PROFINDER (Agilent Technologies). Relative metabolites abundance was carried out after normalization to cell number and statistical analyses were performed using METABOANALYST 5.0 [52].

Bioenergetics by Seahorse technology

Mitochondrial oxygen consumption rate (OCR) and extracellular acidification rate (ECAR) were determined by using Seahorse XFe96 Analyser (Agilent Technologies). Cells were seeded in Agilent Seahorse cell culture microplates at a density of 7–12 × 10^4 cells/well, 24 h prior to the assay and then analysed by using the Seahorse XF ATP rate assay kit (Agilent Technologies), according to manufacturer instructions. At least three measurements of OCR and ECAR were taken for the baseline and after the sequential injection of mitochondrial inhibitors (1.5 µM oligomycin and 1.5 µM rotenone/antimycin A). OCR and ECAR from each well were normalized by protein content by using the Bradford assay.

Enantiomeric HPLC analyses

Human induced pluripotent stem cell-derived mature astrocytes (5 sets of samples at different times of differentiation) or human neuroblastoma SH-SY5Y cells (to perform a comparative analysis) were homogenized in 0.1 mL of 0.2 M TCA, sonicated (three cycles, 10 s each) and centrifuged at 13 000 ***g*** for 20 min. Enantiomeric HPLC analyses were performed as in Ref. [53]: briefly, 10 µL of the supernatants were neutralized with NaOH and subjected to pre-column derivatization with 20 µL of 74.5 mM *o*-phthaldialdehyde (OPA) and 30.5 mM *N*-acetyl L-cysteine (NAC) in 50% methanol. Diastereoisomer derivatives were then resolved on a Symmetry C8 reversed-phase column (5 µm, 4.6 × 250 mm; Waters, Milano, Italy) under isocratic conditions (0.1 M sodium acetate buffer, pH 6.2, 1% tetrahydrofuran and 1 $mL{\cdot}min^{-1}$ flow rate).

Each sample was analysed at least three times (in three different HPLC runs). Identification and quantification of D- and L-Ser, D- and L-Asp and Gly were based on retention times and peak areas, compared with those associated with external standards. The identity of D-Ser and D-Asp peaks was further confirmed by their selective degradation catalysed by wild-type or M213R RgDAAO variants, respectively [54], following the good practices reported in Ref. [55]. The total amount of D- and L-amino acids in cell extracts was normalized by the total protein content of the TCA precipitated protein pellets, which was determined by the Bradford assay after their resolubilization in 1% SDS.

For analysis of the culture medium, it was diluted with HCl (25 mM final concentration) and centrifuged at 39 000 ***g*** for 30 min at 4 °C and rapidly frozen at −80 °C before further analysis.

The amount of lactic acid was determined based on the estimation of hydrogen peroxide formation by lactate oxidase (LOX) reaction (coupled with the Amplex UltraRed assay A36006; Thermo Fisher). 10, 25 and 50 µL of the medium at different times of differentiation were used for the assay solution containing 20 µM Amplex UltraRed, 0.05 $U{\cdot}mL^{-1}$ horseradish peroxidase (HRP), 2.5 mM NaN_3, 1 mM FMN and 1 mU of LOX. The fluorescence of the oxidized reagent produced by LOX activity was recorded continuously for 30 h at 25 °C (535 and 590 nm: excitation and emission wavelengths, respectively). A calibration curve was obtained by adding known amounts of H_2O_2 (0.001–10 µM range). Controls with known amounts of lactic acid, without medium samples, without HRP or with HRP 5-fold more concentrated were assayed simultaneously. Furthermore, 1 mM oxalate (LOX inhibitor) was added to verify the specificity of the activity observed.

All statistical analyses were performed with GRAPHPAD PRISM 7.0 using one-way ANOVA, followed by the *post-hoc* Tukey's test. Differences were considered significant when $P \leq 0.05$.

Shotgun mass spectrometry analysis for label-free proteomics

Human induced pluripotent stem cell-derived mature astrocytes at five different days of differentiation (2, 15, 30, 40 and 56) were analysed by a shotgun label-free proteomic approach for the identification and quantification of expressed proteins, essentially as in Ref. [56]. Cell lysis was performed in a urea lysis buffer containing 20 mM HEPES pH 8.0, 8 M urea and proteases and phosphatases inhibitor cocktail. The homogenate was sonicated using an ultrasonic probe in bursts of 20–30 s and centrifuged at 16 060 ***g*** for 15 min at 18 °C to pellet the cell debris [57]. Prior to proteolysis, proteins were reduced with 13 mM dithiothreitol (15 min at 50 °C) and alkylated with 26 mM iodoacetamide (30 min at room temperature). The material was diluted to a final concentration of 1 M urea by addition of 20 mM HEPES, pH 8.0 and digested overnight with sequencing-grade trypsin (Promega, Madison, WI, USA) for 16 h at 37 °C using a protein : enzyme ratio of 20 : 1 in the presence of 1 mM methylamine [58]. The collected peptides were desalted using Zip-Tip C18 before MS analysis as reported in Ref. [59]. NanoHPLC coupled to MS/MS analysis was performed on Dionex UltiMate 3000 directly connected to an Orbitrap Fusion Tribrid mass spectrometer (Thermo Fisher Scientific) by a nanoelectrospray ion source. Peptide mixtures were enriched on 75 µm ID × 150 mm Acclaim PepMap RSLC C18 column and separated employing the LC gradient: 4% ACN in 0.1% formic acid for 3 min, 4–28% ACN in 0.1% formic acid for 130 min, 28–40% ACN in 0.1% formic acid for 20 min, 40–95% ACN in 0.1% formic for 2 min and 95–4% ACN in 0.1% formic acid for 3 min at a flow rate of 0.3 $\mu L \cdot min^{-1}$. MS spectra of eluting peptides were collected over an m/z range of 375–1500 using a resolution setting of 120 000, operating in the data-dependent mode with a cycle time of 3 s between master scans. HCD MS/MS spectra were acquired in Orbitrap at the resolution of 15 000 using a normalized collision energy of 35% and an isolation window of 1.6 m/z. Dynamic exclusion was set to 60 s. Rejection of +1 and unassigned charge states were enabled. The mass spectrometry proteomics data have been deposited to the ProteomeXchange Consortium via the PRIDE [60] partner repository, with the dataset identifier PXD030739.

Database search and protein identification

Raw label-free MS/MS files from Thermo XCALIBUR software (version 4.1; Thermo Fisher) were analysed using MAXQUANT (version 1.6.0.1; Max Planck Institute of Biochemistry, Munchen, Germany) and searched against the Human Uniprot sequence database (release 09.01.2020), essentially as in Ref. [61]. The following parameters were used: initial maximum allowed mass deviation of 15 p.p.m. for monoisotopic precursor ions and 0.5 Da for MS/MS peaks, trypsin enzyme specificity, a maximum of two missed cleavages, carbamidomethyl cysteine as fixed modification, N-terminal acetylation, methionine oxidation, asparagine/glutamine deamidation and serine/threonine/tyrosine phosphorylation as variable modifications. False protein identification rate (1%) was estimated by searching MS/MS spectra against the corresponding reversed-sequence (decoy) database. The minimum required peptide length was set to 7 amino acids and the minimum number of unique peptides supporting protein identification was set to 1. Quantification in MAXQUANT was performed using the built-in label-free quantification (LFQ) algorithms based on extracted ion intensity of precursor ions. Three biological replicates, each one replicated three times, were carried out. Only proteins present and quantified in 100% of the repeats were considered as positively identified in a sample and used for statistical analyses performed by the PERSEUS software module (version 1.5.5.3, www.biochem.mpg.de/mann/tools/). The expression level of astrocyte maturation markers, PP's enzymes and SR protein at each differentiation day was calculated using the built-in LFQ algorithms based on extracted ion intensity of precursor ions [62]. Protein titers were calculated on the basis of the raw spectral protein intensity (without normalization) of the MAXQUANT software output according to Ref. [63]. The abundance of proteins (in %) was calculated as the ratio of their intensity (MS signal) to the sum of all intensities (total MS signal) in each day of differentiation and the concentration (in $mol \cdot g^{-1}$ of total protein) as the ratio of their intensity (MS signal) to the sum of all intensities (total MS signal) and their molar mass (in $g \cdot mol^{-1}$).

Focussing on specific comparisons (Day 15 vs Day 2, Day 30 vs Day 2, Day 40 vs Day 2, Day 56 vs Day 2, Day 40 vs Day 30 and Day 56 vs Day 30), proteins were considered DE if they were present only in one condition or showed significant t-test difference (Student's t-test P-value ≤ 0.05). Bioinformatic analyses were carried out by Panther (release 16.0) [64], DAVID (release 6.8) [65] and CLUEGO software (CYTOSKAPE release 3.8.2) [66] to cluster enriched annotation groups of Biological Processes, Molecular Function and Pathways within the set of identified proteins. Functional grouping was based on the Fisher's exact test P-value ≤ 0.05 and at least 3 counts. Integration between proteomic and metabolomics data was performed by METABOANALYST software R5.0 based on a Fisher's exact test P-value ≤ 0.05 [67]. The topology analysis aimed to evaluate whether a given gene or metabolite plays an important role in a biological response, based on its position within a pathway (pathway impact).

Author contributions

FT, ZM, GM, VR and EM involved in investigation, data curation, formal analysis, writing—review and editing and visualization; BB involved in investigation; SN and FGS involved in investigation, data curation and visualization; AMR involved in investigation and data curation; SS involved in writing—review and editing, and supervision; RR and CB involved in resources and investigation; LP, GT and PC involved in conceptualization, writing—original draft preparation, writing—review and editing, supervision, project administration and funding acquisition.

Acknowledgments

We thank the OMIC facility of the University of Milano for mass spectrometry data acquisition. ZM is a Ph.D. student of the Biotechnology and Life Sciences course at the University of Insubria. This work is dedicated to the memory of Prof. Nadia Canu, who set up the protocol of astrocyte differentiation. This research was funded by a grant from Ministero Università e Ricerca Scientifica PRIN 2017 (2017H4J3AS) to LP (as coordinator) and to GT and PC (as unit responsible).

Conflict of interest

The authors declare no conflict of interest.

Peer review

The peer review history for this article is available at https://www.webofscience.com/api/gateway/wos/peer-review/10.1111/febs.16816.

Data availability statement

The mass spectrometry proteomics data have been deposited to the ProteomeXchange Consortium via the PRIDE [60] partner repository, with the dataset identifier PXD030739. All other raw data reported in this paper will be shared by the lead contacts upon request.

References

1 Azevedo FAC, Carvalho LRB, Grinberg LT, Farfel JM, Ferretti REL, Leite REP, Filho WJ, Lent R & Herculano-Houzel S (2009) Equal numbers of neuronal and nonneuronal cells make the human brain an isometrically scaled-up primate brain. *J Comp Neurol* **513**, 532–541.

2 Zhang Y & Barres BA (2010) Astrocyte heterogeneity: an underappreciated topic in neurobiology. *Curr Opin Neurobiol* **20**, 588–594.

3 Kriegstein A & Alvarez-Buylla A (2009) The glial nature of embryonic and adult neural stem cells. *Annu Rev Neurosci* **32**, 149–184.

4 Allen NJ (2014) Astrocyte regulation of synaptic behavior. *Annu Rev Cell Dev Biol* **30**, 439–463.

5 Chung WS, Clarke LE, Wang GX, Stafford BK, Sher A, Chakraborty C, Joung J, Foo LC, Thompson A, Chen C *et al.* (2013) Astrocytes mediate synapse elimination through MEGF10 and MERTK pathways. *Nature* **504**, 394–400.

6 Macvicar BA & Newman EA (2015) Astrocyte regulation of blood flow in the brain. *Cold Spring Harb Perspect Biol* **7**, 1–15.

7 Verkhratsky A, Steardo L, Parpura V & Montana V (2016) Translational potential of astrocytes in brain disorders. *Prog Neurobiol* **144**, 188–205.

8 Tiwari N, Pataskar A, Péron S, Thakurela S, Sahu SK, Figueres-Oñate M, Marichal N, López-Mascaraque L, Tiwari VK & Berninger B (2018) Stage-specific transcription factors drive astrogliogenesis by remodeling gene regulatory landscapes. *Cell Stem Cell* **23**, 557–571.e8.

9 Lunt SY & Vander Heiden MG (2011) Aerobic glycolysis: meeting the metabolic requirements of cell proliferation. *Annu Rev Cell Dev Biol* **27**, 441–464.

10 Yamasaki M, Yamada K, Furuya S, Mitoma J, Hirabayashi Y & Watanabe M (2001) 3-Phosphoglycerate dehydrogenase, a key enzyme forl-serine biosynthesis, is preferentially expressed in the radial glia/astrocyte lineage and olfactory ensheathing glia in the mouse brain. *J Neurosci* **21**, 7691–7704.

11 Murtas G, Marcone GL, Sacchi S & Pollegioni L (2020) L-serine synthesis via the phosphorylated pathway in humans. *Cell Mol Life Sci* **77**, 5131–5148.

12 Wolosker H, Blackshaw S & Snyder SH (1999) Serine racemase: a glial enzyme synthesizing D-serine to regulate glutamate-N-methyl-D-aspartate neurotransmission. *Proc Natl Acad Sci USA* **96**, 13409–13414.

13 Reid MA, Allen AE, Liu S, Liberti MV, Liu P, Liu X, Dai Z, Gao X, Wang Q, Liu Y *et al.* (2018) Serine synthesis through PHGDH coordinates nucleotide levels by maintaining central carbon metabolism. *Nat Commun* **9**, 5442.

14 Kawakami Y, Yoshida K, Yang JH, Suzuki T, Azuma N, Sakai K, Hashikawa T, Watanabe M, Yasuda K, Kuhara S *et al.* (2009) Impaired neurogenesis in embryonic spinal cord of Phgdh knockout mice, a serine deficiency disorder model. *Neurosci Res* **63**, 184–193.

15 Kim H & Park YJ (2018) Links between serine biosynthesis pathway and epigenetics in cancer metabolism. *Clin Nutr Res* **7**, 153–160.

16 Konno M, Asai A, Kawamoto K, Nishida N, Satoh T, Doki Y, Mori M & Ishii H (2017) The one-carbon metabolism pathway highlights therapeutic targets for gastrointestinal cancer (review). *Int J Oncol* **50**, 1057–1063.
17 Le Douce J, Maugard M, Veran J, Matos M, Jégo P, Vigneron PA, Faivre E, Toussay X, Vandenberghe M, Balbastre Y *et al.* (2020) Impairment of glycolysis-derived l-serine production in astrocytes contributes to cognitive deficits in Alzheimer's disease. *Cell Metab* **31**, 503–517.e8.
18 Maffioli E, Murtas G, Rabattoni V, Badone B, Tripodi F, Iannuzzi F, Licastro D, Nonnis S, Rinaldi AM, Motta Z *et al.* (2022) Insulin and serine metabolism as sex-specific hallmarks of Alzheimer's disease in the human hippocampus. *Cell Rep* **40**, 111271.
19 Molofsky AV, Krenick R, Ullian E, Tsai H, Deneen B, Richardson WD, Barres BA & Rowitch DH (2012) Astrocytes and disease: a neurodevelopmental perspective. *Genes Dev* **26**, 891–907.
20 Escartin C, Galea E, Lakatos A, O'Callaghan JP, Petzold GC, Serrano-Pozo A, Steinhäuser C, Volterra A, Carmignoto G, Agarwal A *et al.* (2021) Reactive astrocyte nomenclature, definitions, and future directions. *Nat Neurosci* **24**, 312–325.
21 Li J, Pan L, Pembroke WG, Rexach JE, Godoy MI, Condro MC, Alvarado AG, Harteni M, Chen YW, Stiles L *et al.* (2021) Conservation and divergence of vulnerability and responses to stressors between human and mouse astrocytes. *Nat Commun* **12**, 1–20.
22 Doetsch F, Caille I, Lim DA, Garcia-Verdugo JM & Alvarez-Buylla A (1999) Subventricular zone astrocytes are neural stem cells in the adult mammalian brain. *Cell* **97**, 703–716.
23 Seri B, García-Verdugo JM, McEwen BS & Alvarez-Buylla A (2001) Astrocytes give rise to new neurons in the adult mammalian hippocampus. *J Neurosci* **21**, 7153–7160.
24 Sá JV, Kleiderman S, Brito C, Sonnewald U, Leist M, Teixeira AP & Alves PM (2017) Quantification of metabolic rearrangements during neural stem cells differentiation into astrocytes by metabolic flux analysis. *Neurochem Res* **42**, 244–253.
25 Zhang Y, Sloan SA, Clarke LE, Caneda C, Plaza CA, Blumenthal PD, Vogel H, Steinberg GK, Edwards MSB, Li G *et al.* (2016) Purification and characterization of progenitor and mature human astrocytes reveals transcriptional and functional differences with mouse. *Neuron* **89**, 37–53.
26 Krejciova Z, Alibhai J, Zhao C, Krencik R, Rzechorzek NM, Ullian EM, Manson J, Ironside JW, Head MW & Chandran S (2017) Human stem cell-derived astrocytes replicate human prions in a PRNP genotype-dependent manner. *J Exp Med* **214**, 3481–3495.
27 Nadadhur AG, Leferink PS, Holmes D, Hinz L, Cornelissen-Steijger P, Gasparotto L & Heine VM (2018) Patterning factors during neural progenitor induction determine regional identity and differentiation potential in vitro. *Stem Cell Res* **32**, 25–34.
28 Bouvier DS, Fixemer S, Heurtaux T, Jeannelle F, Frauenknecht KBM & Mittelbronn M (2022) The multifaceted neurotoxicity of astrocytes in ageing and age-related neurodegenerative diseases: a translational perspective. *Front Physiol* **13**, 814889.
29 Zamanian JL, Xu L, Foo LC, Nouri N, Zhou L, Giffard RG & Barres BA (2012) Genomic analysis of reactive astrogliosis. *J Neurosci* **32**, 6391–6410.
30 Rodríguez JJ, Terzieva S, Olabarria M, Lanza RG & Verkhratsky A (2013) Enriched environment and physical activity reverse astrogliodegeneration in the hippocampus of AD transgenic mice. *Cell Death Dis* **4**, e678.
31 O'Callaghan JP, Brinton RE & McEwen BS (1991) Glucocorticoids regulate the synthesis of glial fibrillary acidic protein in intact and adrenalectomized rats but do not affect its expression following brain injury. *J Neurochem* **57**, 860–869.
32 Labib D, Wang Z, Prakash P, Zimmer M, Smith MD, Frazel PW, Barbar L, Sapar ML, Calabresi PA, Peng J *et al.* (2022) Proteomic alterations and novel markers of neurotoxic reactive astrocytes in human induced pluripotent stem cell models. *Front Mol Neurosci* **15**, 870085.
33 Locasale JW, Grassian AR, Melman T, Lyssiotis CA, Mattaini KR, Bass AJ, Heffron G, Metallo CM, Muranen T, Sharfi H *et al.* (2011) Phosphoglycerate dehydrogenase diverts glycolytic flux and contributes to oncogenesis. *Nat Genet* **43**, 869–874.
34 Pollegioni L & Sacchi S (2010) Metabolism of the neuromodulator D-serine. *Cell Mol Life Sci* **67**, 2387–2404.
35 Pollegioni L, Sacchi S & Murtas G (2018) Human D-amino acid oxidase: structure, function, and regulation. *Front Mol Biosci* **5**, 107.
36 Keller S, Punzo D, Cuomo M, Affinito O, Coretti L, Sacchi S, Florio E, Lembo F, Carella M, Copetti M *et al.* (2018) DNA methylation landscape of the genes regulating D-serine and D-aspartate metabolism in post-mortem brain from controls and subjects with schizophrenia. *Sci Rep* **8**, 10163.
37 Rabattoni V, Pollegioni L, Tedeschi G, Maffioli E & Sacchi S (2021) Cellular studies of the two main isoforms of human D-aspartate oxidase. *FEBS J* **288**, 4939–4954.
38 Koh W, Park M, Chun YE, Lee J, Shim HS, Park MG, Kim S, Sa M, Joo J, Kang H *et al.* (2022) Astrocytes render memory flexible by releasing D-serine and regulating NMDA receptor tone in the hippocampus. *Biol Psychiatry* **91**, 740–752.

39 Kandasamy P, Gyimesi G, Kanai Y & Hediger MA (2018) Amino acid transporters revisited: new views in health and disease. *Trends Biochem Sci* **43**, 752–789.

40 Foster AC, Farnsworth J, Lind GE, Li YX, Yang JY, Dang V, Penjwini M, Viswanath V, Staubli U & Kavanaugh MP (2016) D-serine is a substrate for neutral amino acid transporters ASCT1/SLC1A4 and ASCT2/SLC1A5, and is transported by both subtypes in rat hippocampal astrocyte cultures. *PLoS One* **11**, e0156551.

41 Powell CL, Davidson AR & Brown AM (2020) Universal glia to neurone lactate transfer in the nervous system: physiological functions and pathological consequences. *Biosensors* **10**, 183.

42 Bak LK, Schousboe A & Waagepetersen HS (2006) The glutamate/GABA-glutamine cycle: aspects of transport, neurotransmitter homeostasis and ammonia transfer. *J Neurochem* **98**, 641–653.

43 Phatnani H & Maniatis T (2015) Astrocytes in neurodegenerative disease. *Cold Spring Harb Perspect Biol* **7**, 1–18.

44 Huang X, Kong H, Tang M, Lu M, Ding JH & Hu G (2012) D-serine regulates proliferation and neuronal differentiation of neural stem cells from postnatal mouse forebrain. *CNS Neurosci Ther* **18**, 4–13.

45 Nuzzo T, Sacchi S, Errico F, Keller S, Palumbo O, Florio E, Punzo D, Napolitano F, Copetti M, Carella M *et al.* (2017) Decreased free D-aspartate levels are linked to enhanced D-aspartate oxidase activity in the dorsolateral prefrontal cortex of schizophrenia patients. *NPJ Schizophr* **3**, 16.

46 Piubelli L, Pollegioni L, Rabattoni V, Mauri M, Princiotta Cariddi L, Versino M & Sacchi S (2021) Serum D-serine levels are altered in early phases of Alzheimer's disease: towards a precocious biomarker. *Transl Psychiatry* **11**, 77.

47 Ito T, Hayashida M, Kobayashi S, Muto N, Hayashi A, Yoshimura T & Mori H (2016) Serine racemase is involved in D-aspartate biosynthesis. *J Biochem* **160**, 345–353.

48 Pollegioni L, Molla G, Sacchi S & Murtas G (2021) Human D-aspartate oxidase: a key player in D-aspartate metabolism. *Front Mol Biosci* **8**, 689719.

49 Baier MP, Nagaraja RY, Yarbrough HP, Owen DB, Masingale AM, Ranjit R, Stiles MA, Murphy A, Agbaga MP, Ahmad M *et al.* (2022) Selective ablation of Sod2 in astrocytes induces sex-specific effects on cognitive function, D-serine availability, and astrogliosis. *J Neurosci* **42**, 5992–6006.

50 Wang C, Wan X, Yu T, Huang Z, Shen C, Qi Q, Xiang S, Chen X, Arbely E, Ling ZQ *et al.* (2020) Acetylation stabilizes phosphoglycerate dehydrogenase by disrupting the interaction of E3 ligase RNF5 to promote breast tumorigenesis. *Cell Rep* **32**, 108021.

51 Tripodi F, Badone B, Vescovi M, Milanesi R, Nonnis S, Maffioli E, Bonanomi M, Gaglio D, Tedeschi G & Coccetti P (2020) Methionine supplementation affects metabolism and reduces tumor aggressiveness in liver cancer cells. *Cells* **9**, 2491.

52 Pang Z, Chong J, Zhou G, De Lima Morais DA, Chang L, Barrette M, Gauthier C, Jacques PÉ, Li S & Xia J (2021) MetaboAnalyst 5.0: narrowing the gap between raw spectra and functional insights. *Nucleic Acids Res* **49**, W388–W396.

53 Punzo D, Errico F, Cristino L, Sacchi S, Keller S, Belardo C, Luongo L, Nuzzo T, Imperatore R, Florio E *et al.* (2016) Age-related changes in D-aspartate oxidase promoter methylation control extracellular D-aspartate levels and prevent precocious cell death during brain aging. *J Neurosci* **36**, 3064–3078.

54 Sacchi S, Lorenzi S, Molla G, Pilone MS, Rossetti C & Pollegioni L (2002) Engineering the substrate specificity of D-amino-acid oxidase. *J Biol Chem* **277**, 27510–27516.

55 Mothet JP, Billard JM, Pollegioni L, Coyle JT & Sweedler JV (2019) Investigating brain D-serine: advocacy for good practices. *Acta Physiol (Oxf)* **226**, e13257.

56 Vernocchi V, Morselli MG, Varesi S, Nonnis S, Maffioli E, Negri A, Tedeschi G & Luvoni GC (2014) Sperm ubiquitination in epididymal feline semen. *Theriogenology* **82**, 636–642.

57 Nicastro R, Tripodi F, Gaggini M, Castoldi A, Reghellin V, Nonnis S, Tedeschi G & Coccetti P (2015) Snf1 phosphorylates adenylate cyclase and negatively regulates protein kinase A-dependent transcription in *Saccharomyces cerevisiae*. *J Biol Chem* **290**, 24715–24726.

58 Eberini I, Calabresi L, Wait R, Tedeschi G, Pirillo A, Puglisi L, Sirtori CR & Gianazza E (2002) Macrophage metalloproteinases degrade high-density-lipoprotein-associated apolipoprotein A-I at both the N- and C-termini. *Biochem J* **362**, 627–634.

59 Mortarino M, Tedeschi G, Negri A, Ceciliani F, Gottardi L, Maffeo G & Ronchi S (1998) Two-dimensional polyacrylamide gel electrophoresis map of bull seminal plasma proteins. *Electrophoresis* **19**, 797–801.

60 Vizcaíno J, Csordas A, Del-Toro N, Dianes J, Griss J, Lavidas I, Mayer G, Perez-Riverol Y, Reisinger F, Ternent T *et al.* (2016) 2016 update of the PRIDE database and its related tools. *Nucleic Acids Res* **44**, 11033.

61 Nonnis S, Maffioli E, Zanotti L, Santagata F, Negri A, Viola A, Elliman S & Tedeschi G (2016) Effect of fetal bovine serum in culture media on MS analysis of mesenchymal stromal cells secretome. *EuPA Open Proteom* **10**, 28–30.

62 Migliaccio O, Pinsino A, Maffioli E, Smith AM, Agnisola C, Matranga V, Nonnis S, Tedeschi G, Byrne M, Gambi MC *et al.* (2019) Living in future ocean acidification, physiological adaptive responses of the immune system of sea urchins resident at a CO_2 vent system. *Sci Total Environ* **672**, 938–950.
63 Wiśniewski JR & Mann M (2016) A proteomics approach to the protein normalization problem: selection of unvarying proteins for MS-based proteomics and Western blotting. *J Proteome Res* **15**, 2321–2326.
64 Mi H, Muruganujan A & Thomas PD (2013) PANTHER in 2013: modeling the evolution of gene function, and other gene attributes, in the context of phylogenetic trees. *Nucleic Acids Res* **41**, D377–D386.
65 Huang DW, Sherman BT & Lempicki RA (2009) Systematic and integrative analysis of large gene lists using DAVID bioinformatics resources. *Nat Protoc* **4**, 44–57.
66 Bindea G, Mlecnik B, Hackl H, Charoentong P, Tosolini M, Kirilovsky A, Fridman WH, Pagès F, Trajanoski Z & Galon J (2009) ClueGO: a Cytoscape plug-in to decipher functionally grouped gene ontology and pathway annotation networks. *Bioinformatics* **25**, 1091–1093.
67 Pang Z, Zhou G, Ewald J, Chang L, Hacariz O, Basu N & Xia J (2022) Using MetaboAnalyst 5.0 for LC-HRMS spectra processing, multi-omics integration and covariate adjustment of global metabolomics data. *Nat Protoc* **17**, 1735–1761.

Supporting information

Additional supporting information may be found online in the Supporting Information section at the end of the article.

Table S1. Proteomics analyses on hiPCS-derived astrocytes.

Table S2. List of the potential markers of reactive astrocytes identified in hiPCS-derived astrocytes by LC–MS/MS.

Table S3. Metabolites showing a significant change during astrocyte differentiation, with fold changes and p-values indicated for each comparison (day 15 vs day 2, day 30 vs day 2, day 40 vs day 2, day 56 vs day 2, day 56 vs day 30).

Table S4. Relative quantification of PHGDH, PSAT, PSP and SR proteins in hiPSC-derived astrocytes during differentiation.